Quantum Monte Carlo study of the two-impurity Kondo Hamiltonian

R. M. Fye* and J. E. Hirsch
Department of Physics B-019, University of California, San Diego, La Jolla, California 92093
(Received 21 November 1988; revised manuscript received 26 May 1989)

We investigate the magnetic properties of the Kondo two-impurity Hamiltonian with a recently introduced, essentially exact quantum Monte Carlo technique. We explore in particular the competition between Kondo effect, with Kondo temperature T_K, and Ruderman-Kittel-Kasuya-Yosida (RKKY) interactions, with coupling constant $\mathcal{J}$. We simulate the regimes $|\mathcal{J}| < T_K$ and $|\mathcal{J}| \gtrsim T_K$ for both ferromagnetic and antiferromagnetic $\mathcal{J}$, considering in particular the antiferromagnetic regime $\mathcal{J}/T_K \approx 2.4$ where anomalous behavior is predicted from renormalization-group calculations. Over the entire parameter range, we find that nearby impurity spin-spin correlations initially develop according to a RKKY effective Hamiltonian $H_{\text{eff}} = \mathcal{J}\mathbf{S}_1 \cdot \mathbf{S}_2$ as the temperature is lowered; the correlations then saturate at around the Kondo temperature T_K. This result suggests an analogous picture for the lattice case, with long-range order developing if a "RKKY lattice" transition temperature is reached before Kondo quenching effects set in. We also find no evidence for anomalous staggered susceptibility behavior in the $\mathcal{J}/T_K \approx 2.4$ regime, and give possible explanations for this difference with the renormalization-group results.

I. INTRODUCTION

The behavior of spin correlations in heavy-fermion systems, some of which order magnetically and some of which do not, is still not completely understood.[1] As a step toward the better understanding of this behavior, we consider here the case of two interacting magnetic impurities of the sort which, in a lattice, are considered to be relevant to heavy-fermion behavior. Specifically, we focus on the two-impurity Kondo system, given by the Hamiltonian

$$H = \sum_{\mathbf{k},\sigma} \epsilon_{\mathbf{k}} c^{\dagger}_{\mathbf{k}\sigma} c_{\mathbf{k}\sigma} + J \sum_{m=1}^{2} \mathbf{S}_c(\mathbf{R}_m) \cdot \mathbf{S}_m \ . \tag{1}$$

Here,

$$\mathbf{S}_c(\mathbf{R}_m) = \frac{1}{N} \sum_{\mathbf{k},\mathbf{k}',\sigma,\sigma'} e^{i(\mathbf{k}-\mathbf{k}')\cdot\mathbf{R}_m} c^{\dagger}_{\mathbf{k}\sigma} \left(\tfrac{1}{2}\boldsymbol{\sigma}_{\sigma\sigma'}\right) c_{\mathbf{k}'\sigma'} \tag{2}$$

is the normalized conduction electron spin localized at $\mathbf{R}_m$, with N the number of different $\mathbf{k}$ vectors, and $\mathbf{S}_m = \frac{1}{2}\boldsymbol{\sigma}_m$ refers to the spin of the magnetic impurity at $\mathbf{R}_m$. In addition, we also consider two Anderson impurities for comparison, with the Hamiltonian

$$H = \sum_{\mathbf{k},\sigma} \epsilon_{\mathbf{k}} c^{\dagger}_{\mathbf{k}\sigma} c_{\mathbf{k}\sigma} + \frac{V}{\sqrt{N}} \sum_{\mathbf{k},m,\sigma} \left(e^{i\mathbf{k}\cdot\mathbf{R}_m} c^{\dagger}_{\mathbf{k}\sigma} f_{m\sigma} + \text{H.c.}\right) + \epsilon_f \sum_{\sigma,m} n_{fm\sigma} + U \sum_{m} n_{fm\uparrow} n_{fm\downarrow} \ . \tag{3}$$

Here, $f_{m\sigma}$ refers to an impurity state of spin σ at site $\mathbf{R}_m$ (again, $m = 1,2$). As we review later, the Kondo Hamiltonian can be derived from the more fundamental Anderson Hamiltonian in the large-U limit.

Because we consider only two impurities rather than a lattice, coherence effects will be missed. However, the two-impurity Hamiltonian contains both Ruderman-Kittel-Kasuya-Yosida (RKKY) interaction effects,[2] which will tend to "order" the two impurity spins into a singlet or triplet, and the Kondo effect, which will presumably try to break that "ordering." These latter two effects are generally thought to be the two most important factors in determining the magnetic properties of heavy-fermion systems, and we thus expect our results to have some relevance to magnetic properties of the lattice.

Earlier scaling work[3] on the two-impurity systems suggested regimes where either Kondo or RKKY effects would be expected to dominate. If the Kondo temperature T_K was much greater than the magnitude of the RKKY coupling $\mathcal{J}$, the impurity spins would be individually Kondo quenched. If $\mathcal{J} \gg T_K$ (antiferromagnetic case), the spins would condense into a two-body singlet before they could be Kondo quenched. However, if $\mathcal{J} < 0$ (ferromagnetic case) and $|\mathcal{J}| \gg T_K$, a two-stage Kondo quenching was indicated. As the temperature was lowered, the spins would first lock into an almost pure triplet, losing one of the four possible degrees of freedom of the two-spin system. The remaining degrees of freedom would then be quenched at two new Kondo temperatures, with spin $1 \rightarrow$ spin-$\frac{1}{2}$ quenching followed by spin $\frac{1}{2} \rightarrow$ spin 0, through conduction electron channels even and odd around the midpoint of the two impurities.

Quantum Monte Carlo studies were done on the two-impurity Anderson system,[4] for the ferromagnetic case $|\mathcal{J}| \lesssim T_K$ and the antiferromagnetic case $\mathcal{J} \ll T_K$. It was found that spin correlations developed according to a RKKY effective Hamiltonian ($H_{\text{eff}} = \mathcal{J}\mathbf{S}_1 \cdot \mathbf{S}_2$) approximately down to the Kondo temperature, at which point they ceased further development. One can picture this qualitatively as Kondo spin fluctuations beginning to dominate thermal spin fluctuations around the Kondo temperature; then, regarding impurity spin correlations, the system would be effectively at temperature T_K for all

$T < T_K$. If the RKKY coupling was ferromagnetic, the normalized uniform susceptibility was enhanced and the staggered susceptibility the same as, or slightly deenhanced, when compared to single-impurity susceptibility values. Because of the small $\mathcal{J}/T_K$ ratio, the trend was difficult to distinguish for antiferromagnetic RKKY coupling. However, in that case, the staggered susceptibility appeared slightly enhanced over the uniform susceptibility.

In addition to extending the parameter regime studied, one of the purposes of this paper is to examine to what extent these findings for the Anderson model are affected by charge fluctuations. Thus, we study here mainly the Kondo Hamiltonian of Eq. (1), where charge fluctuations are eliminated at the outset. (Some new results for the Anderson Hamiltonian are also presented.) This also allows a more direct comparison with recent renormalization-group[5] and auxiliary boson[6] studies of the two-impurity Kondo Hamiltonian.

The renormalization-group work,[5] done for the particle-hole symmetric case, was in qualitative agreement with the Monte Carlo results for the two-impurity Anderson model in terms of spin-correlation development. In addition, a new anomalous fixed point was predicted at antiferromagnetic $\mathcal{J} \approx (2.4) T_K$; here, the staggered susceptibility and the specific-heat coefficient γ were predicted to diverge, leading to a vanishing Wilson ratio. However, an auxiliary boson mean-field theory,[6] gives no divergence in the staggered susceptibility. Rather, in the symmetric case, a discontinuity as a function of $\mathcal{J}/T_K$ can appear in the ground-state staggered susceptibility.

Both of these differing predictions, however, rely upon approximations which have not been shown to be controlled. The two-impurity renormalization-group procedure involves a so-called "energy-independent coupling constant approximation,"[7] which was not used in Wilson's original single-impurity work.[8] The auxiliary boson theory captures basic Kondo effects; however, there is no guarantee that it can reliably treat the interplay between Kondo effect and RKKY interactions. Thus, it is of interest to explore the two-impurity Kondo Hamiltonian with a controlled and essentially exact technique.

The technique that we use is a variant of the fermion algorithm recently introduced to study interacting Anderson impurities in metals.[9,10] Here, we first apply a projector operator to turn the fermion impurities into spins by projecting out doubly occupied and unoccupied impurity states. As before, we then use the Trotter approximation to isolate the interaction terms of the Hamiltonian, giving an approximate partition function whose behavior is now well understood.[11,12] We next decouple the interaction terms using generalized discrete Hubbard-Stratonovitch transformations,[13] leaving the partition function in bilinear fermion form in a fluctuating Ising field. Finally, we perform Monte Carlo simulations of the Ising field, calculating the fermion trace at each step and measuring the desired quantities. We refer the interested reader to Appendix A for a more detailed discussion of the methodological aspects specific to this calculation, and to Refs. 9 and 10 for a more general discussion.

After the simulations, we extrapolate in the expansion parameter $(\Delta\tau)^2$ to achieve results exact to within a few percent.[11,12] As an example, in Fig. 1 we compare Monte Carlo and exact results for a system of two Kondo (spin) impurities and two conduction-electron sites. The Monte Carlo results here are roughly extrapolated from two values of $\Delta\tau$. Unless otherwise stated, error bars in all figures include estimates of statistical error plus extrapolation uncertainty.

We focus in this paper on the impurity spin correlation $\langle \sigma_{z1}\sigma_{z2} \rangle$ (which can range from -1 to $\frac{1}{3}$), the on-site magnetic susceptibility

$$\chi = \int_0^\beta d\tau \langle \sigma_{z1}(\tau)\sigma_{z1} \rangle , \tag{4}$$

the normalized uniform susceptibility

$$\chi^{(u)} = \tfrac{1}{2}\int_0^\beta d\tau \langle [\sigma_{z1}(\tau)+\sigma_{z2}(\tau)][\sigma_{z1}+\sigma_{z2}] \rangle , \tag{5}$$

and the normalized staggered susceptibility

$$\chi^{(s)} = \tfrac{1}{2}\int_0^\beta d\tau \langle [\sigma_{z1}(\tau)-\sigma_{z2}(\tau)][\sigma_{z1}-\sigma_{z2}] \rangle . \tag{6}$$

Our algorithm can also be used to calculate differences between extensive quantities of virtually infinite systems with essentially no algorithmic dependence on system size. Thus, we could, for example, measure an impurity coefficient of specific heat γ. However, this involves an order of magnitude or so more computer time, so that we defer such studies to a later date.

We begin in Sec. II by discussing the relationship between the two-impurity Kondo and Anderson systems, followed in Sec. III by a discussion of expected results in limiting cases. We then give results for antiferromagnetic RKKY interactions in Sec. IV, followed in Sec. V by results for ferromagnetic RKKY interactions. In Sec. VI

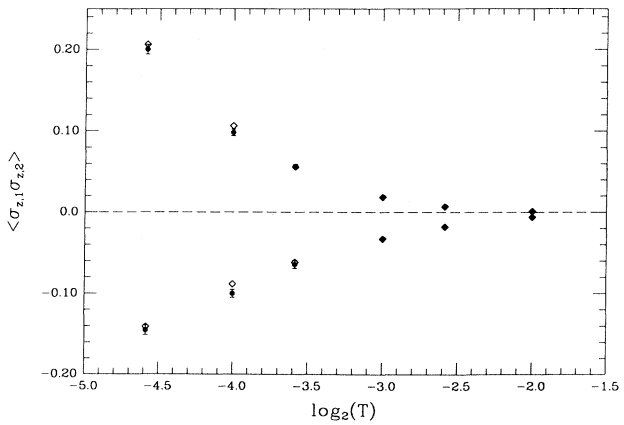

FIG. 1. $\langle \sigma_{z1}\sigma_{z2} \rangle$ vs $\log_2(T)$ for two Kondo impurities on two sites with "conduction electron" hopping between the sites [i.e., two-site version of Eq. (25)]. $t = \frac{1}{2}$, $J = 1.0$, $\mu_c = 0.0$ (bottom), and $\mu_c = -0.5$ (top). Monte Carlo (solid circles) and exact diagonalization (open diamonds).

we explore the dependence of the spin correlations on interimpurity distance, and in Sec. VII we consider the crossover behavior from small to large J, where, for example, correlations can change from ferromagnetic to antiferromagnetic as a function of J. Finally, we summarize our conclusions in Sec. VIII.

II. RELATIONSHIP BETWEEN KONDO AND ANDERSON TWO-IMPURITY HAMILTONIANS

A. Kondo behavior

We begin by comparing the Anderson and Kondo single-impurity Hamiltonians, in order to relate the Kondo-quenching behavior of the two systems. [Single-impurity Hamiltonians can be obtained by taking only $m=1$ in Eqs. (1) and (3), and then setting $\mathbf{R}_1=0$ for simplicity.] We consider first the case in which the Coulomb repulsion U is much greater than the conduction electron bandwidth D, and then the case where $D \gg U$.

For $U \gg D$, the Schrieffer-Wolff transformation[14] shows that the two single-impurity Hamiltonians are equivalent, with the same conduction-electron band structures, if $J=8V^2/U$ in the symmetric case $\epsilon_f + U/2 = 0$ (related results hold in the near-symmetric, non-valence-fluctuating regime). To test the approach to this equivalence, we show in Fig. 2 with open diamonds $T\chi$ versus $\log_2(T)$ for a single Kondo impurity with $J=1.0$, a conduction band extending from -1 to 1 ($D=2$), a chemical potential $\mu_c=0$, and a flat single-particle density of states $\rho=\frac{1}{2}$. We also show on the same graph symmetric Anderson impurity results for $T\chi$, with $8V^2/U=1.0$; $U=1$, 4, and 16; and the same conduction-band structure. It is clear that the magnetic behaviors of the two systems approach each other as U increases, becoming equal here to within a few percent at $U \sim 8D$.

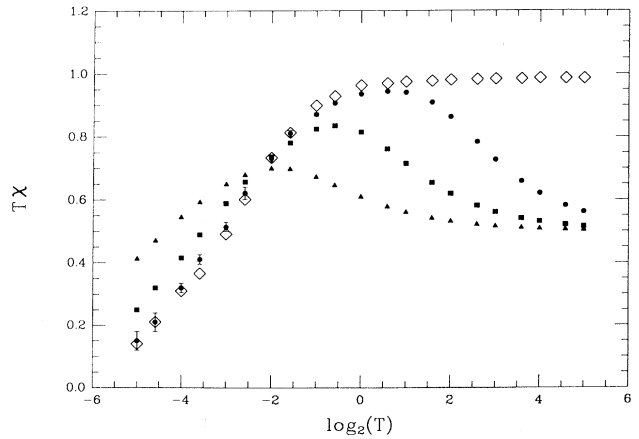

FIG. 2. T_χ vs $\log_2(T)$ for single Kondo and Anderson impurities. Bandwidth is from -1 to 1, with flat single-particle density of states $\rho=\frac{1}{2}$ and $\mu_c=0.0$. Kondo impurity, $J=1.0$, open diamonds. All Anderson impurities, $8V^2/U=1.0$. $U=1$, solid triangles; $U=4$ solid squares; $U=16$, solid circles. Errors, if not shown, are less than or equal to symbol size.

In the opposite limit, $D \gg U$, charge excitation processes rather than the conduction band itself provide an effective band cutoff for the Anderson model,[15] so that the band structures of the two equivalent Kondo and Anderson systems are different. For small ρJ, where ρ is the single-particle density of states at the Fermi surface,

$$T_K \approx D(\rho J)^{1/2} e^{-1/\rho J} \tag{7}$$

for a Kondo impurity.[8] For an Anderson impurity,

$$T_K \approx D_{\text{eff}}(\rho J)^{1/2} e^{-1/\rho J} , \tag{8}$$

where again

$$J=\frac{8V^2}{U} ; \tag{9}$$

however, $D_{\text{eff}}=(0.182)U$.[15] The relationship between Kondo and Anderson impurity systems in this $D \gg U$ limit has been explored in some detail using renormalization-group techniques,[16] the Bethe ansatz,[17] and quantum Monte Carlo techniques.[10]

B. RKKY behavior

When $U \gg D$, the RKKY interactions between two Kondo and Anderson impurities become identical, with the same conduction-band structure in both cases, when $J=8V^2/U$. Thus, since both Kondo quenching and RKKY interaction effects are identical, we expect all Anderson two-impurity systems with $U \gg D, V^2/U$ constant, and a given band structure to map onto the same Kondo two-impurity system once a local moment develops, with $J=8V^2/U$ and the same conduction-band structure.

When $D \gg U$, the RKKY interactions in the two systems are not made equivalent simply by setting $J=8V^2/U$; as in the single-impurity case, the Schrieffer-Wolff relationship between the two systems becomes more complicated. It may be possible that using an effective cutoff $D \sim U$, along with $J=8V^2/U$, would restore RKKY equivalence; we do not explore that here. Rather, we simply choose to perturbatively calculate a T_K and a RKKY $\mathcal{J}$ for whatever system we are studying, and then to try to understand the behavior in terms of these two calculated parameters.

III. EXPECTED LIMITS

A. $T_K \gg |\mathcal{J}|$: $\mathcal{J}$ either ferromagnetic or antiferromagnetic

For $T_K < T \ll D$, we expect correlations to develop according to the RKKY effective Hamiltonian as

$$\langle \sigma_{z1}\sigma_{z2} \rangle = \frac{1-e^{\beta\mathcal{J}}}{3+e^{\beta\mathcal{J}}} \tag{10}$$

$$\approx -\frac{\beta\mathcal{J}}{4} . \tag{11}$$

We then expect the correlations to stop development and saturate at $T \sim T_K$.

For susceptibilities, we again refer to the RKKY effective Hamiltonian. From that Hamiltonian by itself,

with $T \gg \mathcal{J}$, we have for the "effective uniform moment"

$$T\chi^{(u)} \approx T\chi \left[1 - \frac{\beta \mathcal{J}}{4} \right] \tag{12}$$

and for the "effective staggered moment"

$$T\chi^{(s)} \approx T\chi \left[1 + \frac{\beta \mathcal{J}}{4} \right] , \tag{13}$$

where χ is the on-site susceptibility [Eq. (4)] of the two-spin RKKY system. We might then expect the forms of Eqs. (12) and (13) to hold also in the Kondo case, where χ in Eqs. (12) and (13) was now the on-site susceptibility of the two-impurity Kondo system ($T\chi$ being the "effective moment"). In further analogy with the spin correlations, we would expect all susceptibilities to saturate at $T \sim T_K$.

If the Kondo two-impurity on-site and the one-impurity susceptibilities were the same through order $\mathcal{J}$, χ in Eqs. (12) and (13) could then refer to the single-impurity susceptibility. However, if those two susceptibilities differ in order $\mathcal{J}$, the more general parametrization

$$T\chi^{(u)} \approx T\chi \left[1 - (1+\alpha) \frac{\beta \mathcal{J}}{4} \right] \tag{14}$$

and

$$T\chi^{(s)} \approx T\chi \left[1 + (1-\alpha) \frac{\beta \mathcal{J}}{4} \right] \tag{15}$$

would be expected, where χ in Eqs. (14) and (15) is now the Kondo single-impurity susceptibility and α is some constant. As before, we would expect all susceptibilities to saturate at $T \sim T_K$.

B. $\mathcal{J} \gg T_K$ (antiferromagnetic case)

As before, for $T \ll D$, we expect correlations to develop according to an RKKY effective Hamiltonian, but to stop development around the Kondo temperature before a pure singlet state is reached (i.e., there will be a small triplet component mixed in the ground state). We also expect the RKKY Hamiltonian by itself to govern susceptibilities, so that, when T becomes much smaller than $\mathcal{J}$,

$$T\chi \to \frac{2T}{\mathcal{J}} , \tag{16}$$

$$T\chi^{(u)} \to (4\beta) e^{-\beta \mathcal{J}} , \tag{17}$$

and

$$T\chi^{(s)} \to \frac{4T}{\mathcal{J}} . \tag{18}$$

For comparison, for a single impurity,

$$T\chi \to \frac{(0.103)T}{T_K} \tag{19}$$

for $T \ll T_K$.[8]

Thus, we see that, for $\mathcal{J} \gg T_K$, all three two-impurity susceptibilities (on site, uniform, and staggered) are expected to be reduced from the single-impurity susceptibility when $T \ll \mathcal{J}$. This is much different from the case $T_K \gg \mathcal{J}$, where we might expect $T\chi^{(s)}$ to be enhanced over the single-impurity T_χ. In essence, for $\mathcal{J} \gg T_K$, the impurity spins are now "RKKY quenched" by forming a two-body singlet before they can enter the many-body Kondo singlet state.

C. $|\mathcal{J}| \gg T_K$ (ferromagnetic case)

Again, we expect two-impurity correlations to follow an RKKY development, but not to achieve a pure triplet state. At temperatures $T_K \ll T \ll \mathcal{J}$, we expect the spins to be in a mostly triplet state, however, so that

$$T\chi \sim \tfrac{2}{3} , \tag{20}$$

$$T\chi^{(u)} \sim \tfrac{4}{3} , \tag{21}$$

and

$$T\chi^{(s)} \sim \frac{4T}{3|\mathcal{J}|} . \tag{22}$$

We expect two new Kondo temperatures, $T_K^{(1)}$ and $T_K^{(2)}$, to be generated.[3] These new temperatures refer to the reduction of the effective two-impurity moment from spin 1 to spin $\frac{1}{2}$, and then from spin $\frac{1}{2}$ to spin 0. Thus, for $T_K^{(2)} \lesssim T \lesssim T_K^{(1)}$, we expect $T\chi \sim \frac{1}{4}$ and $T\chi^{(u)} \sim \frac{1}{2}$ (as a reminder, $\chi^{(u)}$ is normalized by dividing by 2). For $T \lesssim T_K^{(1)}$, we would then expect $2T\chi^{(u)}$ to follow the single-impurity $T\chi$ curve, and $T\chi \sim \frac{1}{2} T\chi^{(u)}$.

IV. ANTIFERROMAGNETIC RKKY INTERACTIONS

A. $\mathcal{J} \ll T_K$

We consider first two nearest-neighbor Kondo impurities on a three-dimensional nearest-neighbor-hopping lattice, with Hamiltonian

$$H = \sum_{\langle i,j \rangle, \sigma} t_{ij} c_{i\sigma}^{\dagger} c_{j\sigma} + J \sum_{m=1}^{2} [\mathbf{S}_c(\mathbf{R}_m) \cdot \mathbf{S}_m] . \tag{23}$$

Here, i and j denote three-dimensional indices, and the $\langle i,j \rangle$ summation refers to all nearest neighbors. We choose $t = \frac{1}{6}$, which gives a conduction band from -1 to 1, with single-particle density of states shown in Fig. 3. We set the chemical potential μ_c equal to 0 (symmetric case), giving a density of states $\rho \approx 0.85$ at the Fermi surface. We pick a large enough system so that size effects are negligible.

In Fig. 4, we show $\langle \sigma_{z1} \sigma_{z2} \rangle$ versus $\log_2(T)$ for $J = 0.5$ ($\rho J \approx 0.43$), as well as the $\langle \sigma_{z1} \sigma_{z2} \rangle$ expected from an RKKY effective Hamiltonian $H_{\text{eff}} = \mathcal{J} \mathbf{S}_1 \cdot \mathbf{S}_2$, with $\mathcal{J}$ computed from the standard lowest-order RKKY formula using this band structure (open diamonds). Also, we show with an arrow on the x axis the Kondo temperature T_K determined from the formula[8]

$$T_K \approx D(\rho J)^{1/2} e^{-1/\rho J} , \tag{24}$$

where we choose $D = 1$ to reflect the density of states (DOS) structure of Fig. 3. This formula of Eq. (24) is per-

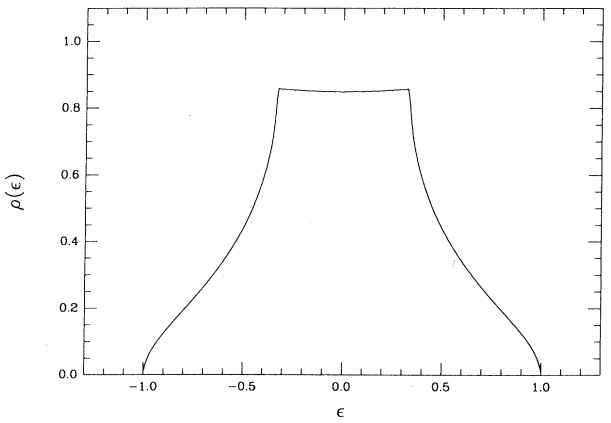

FIG. 3. Density of states for three-dimensional nearest-neighbor-hopping lattice, with t set to $\frac{1}{6}$.

turbative in ρJ, and we do not expect it to be quantitatively accurate for the values of ρJ investigated in this paper. However, it still serves as a useful guideline.

Thus, we see that spin correlations initially develop for $T \ll D$ according to a RKKY effective Hamiltonian, though they are slightly reduced in magnitude from the RKKY prediction due to the neglect of RKKY perturbative terms of higher order than $(\rho J)^2$. At around the Kondo temperature T_k, the correlations then appear to level off and saturate.

In Fig. 5, we show $T\chi^{(s)}$, $T\chi$, and $T\chi^{(u)}$ versus $\log_2(T)$. We also measured $T\chi$ for a single impurity; it is indistinguishable here from $T\chi$ for the two-impurity system, which suggests that α in Eqs. (14) and (15) is 0 (or, at least, very small) for $\mathcal{J}$ antiferromagnetic. With α set to 0, we find that Eqs. (14) and (15) describe the susceptibilities within statistical error for $T > T_K$, with saturation beginning to set in for $T < T_K$.

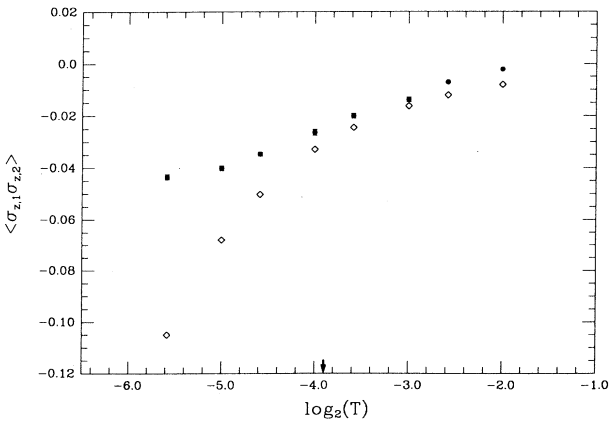

FIG. 4. $\langle \sigma_{z1}\sigma_{z2} \rangle$ vs $\log_2(T)$ for Kondo nearest neighbors on three-dimensional nearest-neighbor-hopping lattice, with $t=\frac{1}{6}$, $J=\frac{1}{2}$, and $\mu_c=0.0$. Monte Carlo data, solid circles; RKKY predictions, open diamonds.

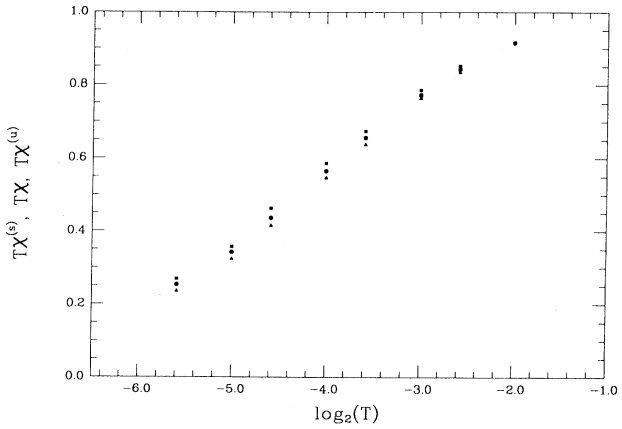

FIG. 5. From top to bottom, $T\chi^{(s)}$ (solid squares), $T\chi$ (solid circles), and $T\chi^{(u)}$ (solid triangles) vs $\log_2(T)$ for same parameters as Fig. 4. Errors are less than or equal to symbol size. $T\chi$ for a single impurity (not explicitly shown) is here indistinguishable from $T\chi$ for the two-impurity system.

B. $\mathcal{J} > T_K$

We now consider two nearest-neighbor impurities on a one-dimensional lattice,

$$H = t\sum_{i,\sigma}(c^{\dagger}_{i,\sigma}c_{i+1,\sigma} + \text{H.c.}) + J\sum_{m=1}^{2}[\mathbf{S}_c(\mathbf{R}_m)\cdot\mathbf{S}_m] , \qquad (25)$$

where it is easier for us to achieve a large $\mathcal{J}/T_K$ ratio. We set $t=\frac{1}{2}$, giving a band from -1 to 1, with single-particle density of states shown in Fig. 6. Again, we set $\mu_c=0.0$ (symmetric case), giving a DOS $\rho = 1/\pi \approx 0.32$ at the Fermi surface.

We choose first $J=0.8$ ($\rho J \approx 0.26$), giving an RKKY $\mathcal{J} \approx 0.044$. Setting $D=2$, we find from Eq. (24) that $T_K \approx 0.020$, so that $\mathcal{J}/T_K \approx 2.2$. Thus, we should be close to the predicted "anomalous fixed point" ratio for $\mathcal{J}/T_K$, with a similar value of ρJ[5,7] (though a different band structure), where the staggered susceptibility is predicted to diverge.

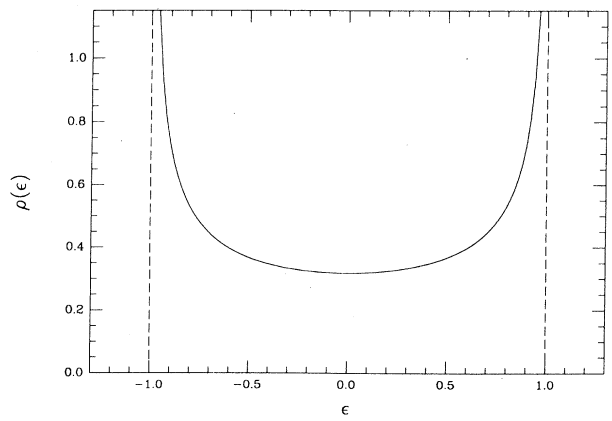

FIG. 6. Density of states for one-dimensional nearest-neighbor-hopping lattice, with t set to $\frac{1}{2}$.

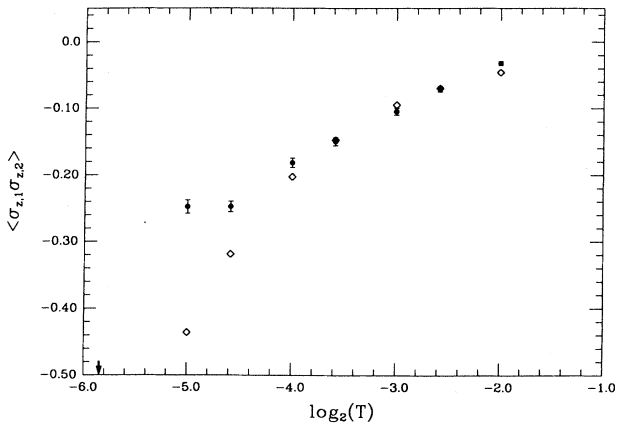

FIG. 7. $\langle \sigma_{z1}\sigma_{z2} \rangle$ vs $\log_2(T)$ for Kondo nearest neighbors on one-dimensional nearest-neighbor-hopping lattice, with $t=\frac{1}{2}$, $J=0.8$, and $\mu_c=0.0$. Solid circles, Monte Carlo data. Open diamonds, RKKY predictions. T_K shown by arrow.

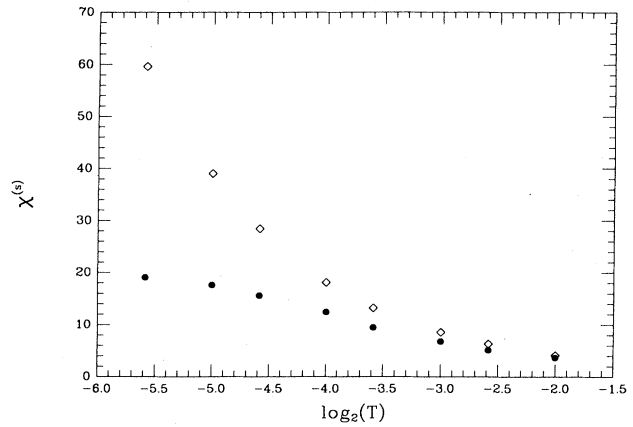

FIG. 9. $\chi^{(s)}$ vs $\log_2(T)$ from Monte Carlo data (solid circles) and RKKY effective Hamiltonian (open diamonds). Spins are Kondo nearest neighbors on one-dimensional hopping lattice with $t=\frac{1}{2}$, $J=0.728$, and $\mu_c=0.0$. $\chi^{(s)}$ from the RKKY effective Hamiltonian saturates at $\chi^{(s)}\approx 110$ when $\beta\approx 192$.

In Fig. 7, we show $\langle \sigma_{z1}\sigma_{z2} \rangle$ versus $\log_2(T)$, as well as the $\langle \sigma_{z1}\sigma_{z2} \rangle$ expected from the RKKY $H_{\text{eff}}=\mathcal{J}\mathbf{S}_1\cdot\mathbf{S}_2$ with $\mathcal{J}$ calculated using this band structure. We see that correlations are well described by the effective Hamiltonian down to $\beta\approx 16$; then, they begin to level off and saturate at $\langle \sigma_{z1}\sigma_{z2} \rangle \approx -0.25$, which may be compared with the value $\langle \sigma_{z1}\sigma_{z2} \rangle \approx -0.33$ for the "anomalous fixed point" of Refs. 5 and 7.

In Fig. 8, we show $T\chi^{(s)}$, $T\chi$, and $T\chi^{(u)}$ for the two-impurity system, as well as $T\chi$ for the single-impurity case (open diamonds). As the temperature is lowered, we begin to see the effect predicted earlier for $\mathcal{J} \gg T_K$, in which all three two-impurity susceptibilities lie below the single-impurity susceptibility. We thus expect the ground-state staggered susceptibility here to be slightly less than the single-impurity susceptibility, and therefore to have no anomalously high value or divergence.

To further investigate the renormalization-group predictions, we next choose $J=0.728$ ($\rho J\approx 0.232$), giving $\mathcal{J}\approx 0.0362$, $T_K\approx 0.0129$, and $\mathcal{J}/T_K\approx 2.8$. We find that this value of J gives a saturated spin correlation $\langle \sigma_{z1}\sigma_{z2} \rangle \approx -0.33$, the same as the ground-state renormalization-group correlation at the predicted "anomalous fixed point" $\mathcal{J}/T_K$ ratio.

In Fig. 9, we show $\chi^{(s)}$ versus $\log_2(T)$ for this $\rho J\approx 0.232$, as well as the $\chi^{(s)}$ predicted from an RKKY effective Hamiltonian with $\mathcal{J}\approx 0.0362$. We see that $\chi^{(s)}$ appears to be beginning to saturate at $\beta\approx 48$, and is much reduced due to Kondo quenching from the RKKY Hamiltonian value, which saturates at $\chi^{(s)}_{\text{RKKY}}\approx 110$ when $\beta\approx 192$. Again, we see no suggestion of unusual behavior.

For completeness, we then consider in addition two other values of J, $J=0.96$ ($\rho J\approx 0.307$) and $J=1.32$ ($\rho J\approx 0.422$), giving $\mathcal{J}/T_K\approx 1.5$ and $\mathcal{J}/T_K\approx 0.9$, respectively. We show in Fig. 10 $\chi^{(s)}$ versus $\log_2(T)$ for, from top to bottom, $\rho J\approx 0.232$ ($\mathcal{J}/T_K\approx 2.8$), $\rho J\approx 0.256$ ($\mathcal{J}/T_K\approx 2.2$), $\rho J\approx 0.307$ ($\mathcal{J}/T_K\approx 1.5$), and $\rho J\approx 0.422$ ($\mathcal{J}/T_K\approx 0.9$). It is not impossible that unusual additional structure would emerge at unexpectedly low temperatures. However, comparing Figs. 9 and 10, we see that all the curves have the same general shape when scaled, and all show signs of saturation at low temperature. Thus, we see no indication of unusual behavior, and our data strongly suggest that the staggered susceptibility is always well behaved.

In Fig. 11, lastly, we show $T_K\chi^{(s)}$ versus $\mathcal{J}/T_K$ for these above four values of ρJ, corresponding to Fig. (2) of Ref. 5. Here $\chi^{(s)}$ is measured at $T=\frac{3}{2}T_K$. We would expect this graph to look similar in shape if $\chi^{(s)}$ were measured at $T=0$ rather than $T=\frac{3}{2}T_K$, however, due to the previously mentioned similar scaled shapes of the curves in Fig. 10.

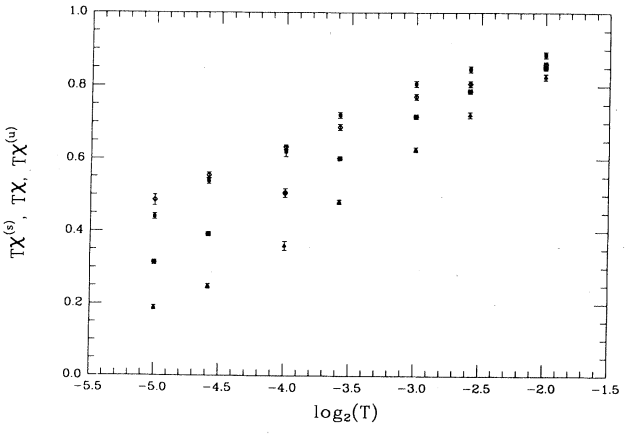

FIG. 8. From top to bottom, solid symbols, $T\chi^{(s)}$ (solid squares), $T\chi$ (solid circles), and $T\chi^{(u)}$ (solid triangles) vs $\log_2(T)$ for same parameters as Fig. 7. Open diamonds, $T\chi$ for a single impurity.

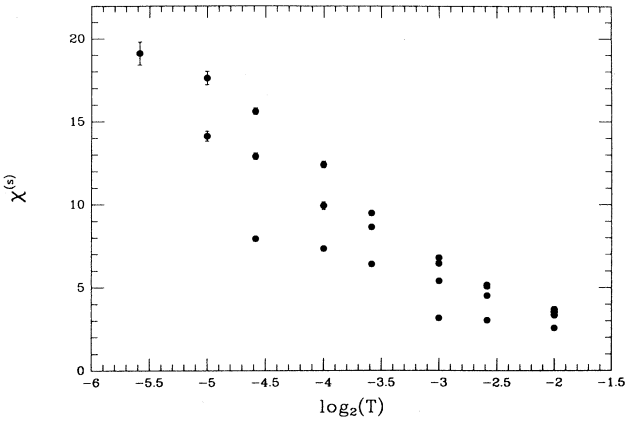

FIG. 10. $\chi^{(s)}$ vs $\log_2(T)$, for Kondo nearest-neighbor spins on one-dimensional hopping lattice with $t=\frac{1}{2}$ and $\mu_c=0.0$. From top to bottom, $J=0.728$, 0.8, 0.96, and 1.32.

Again, we see nothing unusual, such as a divergence at $\mathscr{J}/T_K \approx 2.4$. The "normalized" staggered susceptibility $T_K\chi^{(s)}$ initially goes up for small $\mathscr{J}/T_K$, corresponding to Eq. (15) with $\alpha=0$. It then eventually begins to diminish, presumably approaching $2/\mathscr{J}$ [Eq. (16)] as $\mathscr{J}/T_K \to \infty$.

In essence, we find no staggered susceptibility divergence or other anomalous behavior in the regime predicted by renormalization group results. This may be because we did not exactly hit the predicted fixed point, though we are sufficiently close that some unusual feature should be noticeable.[5,7] Different band structures were used, but it would be surprising if anomalous behavior were limited to one particular structure, and both Monte Carlo and renormalization-group results are for the particle-hole symmetric case. Another possible explanation may be the different definitions of staggered susceptibility; we expect at least the same qualitative behavior for the two definitions, but this has not been made rigorous. A last possibility might be the previously mentioned

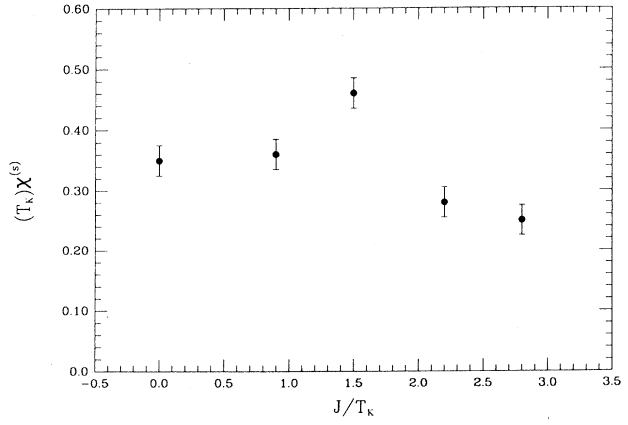

FIG. 11. $TK\chi^{(s)}$ vs $\mathscr{J}/T_K$ with $\chi^{(s)}$ calculated at $T \approx \frac{3}{2}T_K$ from the data of Fig. 10.

"energy-independent coupling approximation" used in the renormalization-group work.[7]

The auxiliary boson mean-field predictions,[6] however, do not appear inconsistent with our results. Though our results suggest a continuous variation of the ground-state staggered susceptibility with $\mathscr{J}/T_K$, a small discontinuity in the susceptibility would not contradict the data of Fig. 11. Nonetheless, we consider it most likely, as suggested in Ref. 6, that fluctuations around the mean-field solution will close the predicted discontinuity. Also, in contrast to the renormalization-group work, both Monte Carlo and auxiliary boson results are for identical definitions of the staggered susceptibility.

V. FERROMAGNETIC RKKY INTERACTIONS

A. $|\mathscr{J}| \ll T_K$

We first consider the case $|\mathscr{J}| \ll T_K$. For this, we choose two impurities on a one-dimensional lattice a distance of four lattice sites apart. As before, we set $t=\frac{1}{2}$ and $\mu_c=0.0$, giving a band from -1 to 1 with $\rho \approx 0.32$ at the Fermi surface. We choose $J=1.0$, giving $\rho J \approx 0.32$.

For reasons which are discussed in Sec. VI, we do not attempt to quantitatively parametrize correlation or susceptibility properties here in terms of the parametrizations of Sec. III. Rather, we are interested in the qualitative effect of a small ferromagnetic RKKY interaction on the various susceptibilities.

In Fig. 12, we show $T\chi^{(u)}$, $T\chi^{(s)}$, and $T\chi$ for the above parameters, as well as $T\chi$ for the corresponding single impurity. In analogy with the antiferromagnetic case, the uniform susceptibility is enhanced and the staggered susceptibility dehanced over the two-impurity on-site susceptibility. However, in contrast to the antiferromagnetic case, the two-impurity on-site susceptibility appears to be similarly enhanced over the single-impurity suscepti-

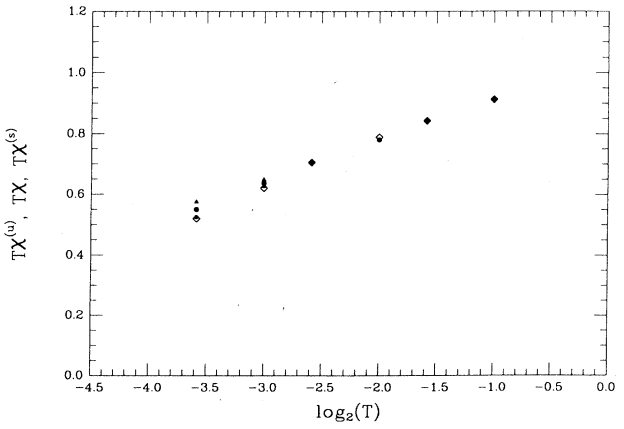

FIG. 12. From top to bottom, solid symbols, $T\chi^{(u)}$ (solid triangles), $T\chi$ (solid circles), and $T\chi^{(s)}$ (solid squares) vs $\log_2(T)$. Open diamonds, $T\chi$ for a single-impurity. $J=1.0$ and Kondo spins are four lattice sites apart on a one-dimensional hopping lattice with $t=\frac{1}{2}$ and $\mu_c=0.0$. Errors are less than or equal to symbol size.

bility. This behavior was also seen in Anderson two-impurity simulations.[4]

These results may be interpreted as a Kondo temperature reduced by a term linear in $\mathcal{J}$. They also suggest that, when Eqs. (14) and (15) (or similar forms) are valid, $\alpha \approx 1$ when $\mathcal{J}$ is ferromagnetic.

B. $|\mathcal{J}| \gtrsim T_K$: Anderson Hamiltonian

For $|\mathcal{J}| > T_K$, we next discuss two Anderson impurities in a three-dimensional electron gas, with Hamiltonian of the form of Eq. (3). We set

$$\epsilon(k) = \frac{D}{2}\left[\left[\frac{k}{k_F}\right]^2 - 1\right], \tag{26}$$

with $0 < k < k_F\sqrt{2}$, and choose $U=3$, $\epsilon_f + U/2 = 0$, and $D=12$, so that we are closer to the $D \gg U$ limit. We also set $k_F R = \frac{1}{2}$, so that the RKKY interaction is ferromagnetic, and choose $\Delta = \pi\rho V^2$ to be $\frac{1}{2}$, where Δ is the approximate width at half maximum of a single-impurity state caused by impurity-conduction hybridization. Previous work[4] was done mostly for $U=2$ and $\Delta = \frac{1}{2}$; however, when $U=3$, so that $U/\Delta = 6$, the Wilson ratio is within a few percent of the (Kondo) impurity value of 2,[18] and moment formation is well described by a large-U Hartree-Fock parametrization.[10] Thus, for $U=3$, we expect behavior to be fully representative of the large-U regime.

In Fig. 13, we show $\langle \sigma_{z1}\sigma_{z2} \rangle$ versus $\log_2(T)$, with the Kondo temperature $T_K \approx 0.044$ shown on the x axis, as well as a fit to a RKKY predicted $\langle \sigma_{z1}\sigma_{z2} \rangle$. (Here, T_K obtained from the Bethe ansatz formula[17,18] is not perturbative.) We thus see that, as in the case when $U=2$,[4] spin correlations develop following a RKKY effective Hamiltonian down to around the Kondo temperature, at which point they are quenched. The lowest-order ground-state perturbative RKKY coupling $\mathcal{J}$ between two Anderson impurities overestimates the correlation

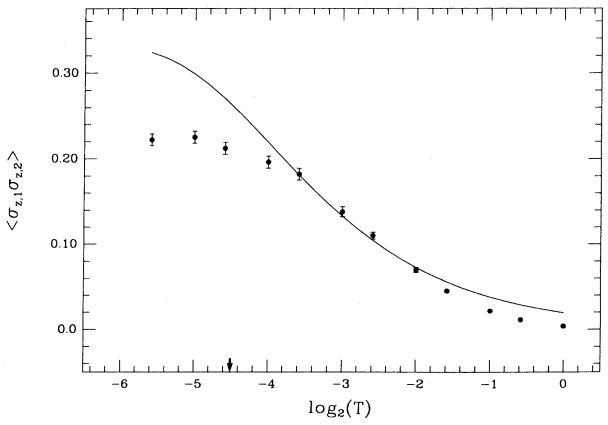

FIG. 13. $\langle \sigma_{z1}\sigma_{z2} \rangle$ vs $\log_2(T)$ for two Anderson impurities in conduction-electron gas. $U=3$, $\Delta = \frac{1}{2}$, $D=12$, $\mu_c = 0.0$, $k_F R = \frac{1}{2}$. T_K shown by arrow.

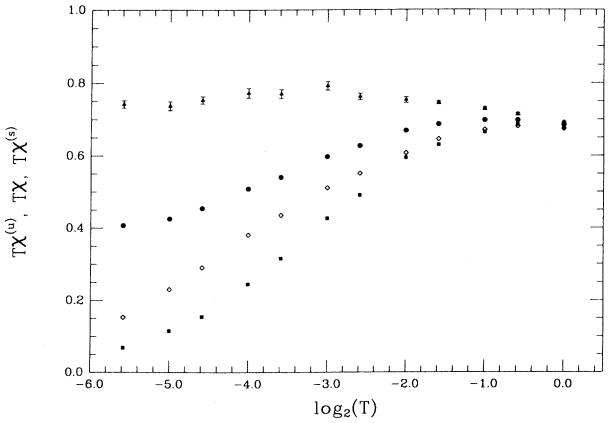

FIG. 14. From top to bottom, solid symbols, $T\chi^{(u)}$ (solid triangles), $T\chi$ (solid circles), and $T\chi^{(s)}$ (solid squares) vs $\log_2(T)$ for same parameters as Fig. 13. Open diamonds, $T\chi$ for a single impurity. Errors, if not shown, are less than or equal to symbol size.

development for $U=3$ (a finite-temperature fit was done in Ref. 4). However, the correlation development can be fit as shown to an effective RKKY $\mathcal{J}'$, where here $\mathcal{J}' \approx -0.067$. In general, $\mathcal{J}$ and $\mathcal{J}'$ converge as U/Δ increases, and join to within a few percent at $U/\Delta \approx 12$.[19]

In Fig. 14, we show, from top to bottom, $T\chi^{(u)}$, $T\chi$, and $T\chi^{(s)}$ for $U=3$, as well as $T\chi$ for a single impurity (open diamonds). If we attempt to use the $|\mathcal{J}| \gg T_K$ limit of Ref. 3, we would expect the ferromagnetically correlated two-spin system to go effectively from spin 1 to spin $\frac{1}{2}$ at $T_K^{(1)} \sim 0.04$, and from spin $\frac{1}{2}$ to spin 0 at $T_K^{(2)} \sim 6\times 10^{-12}$. However, since both T_K and $T_K^{(1)}$ are of order $\mathcal{J}'$, the Kondo quenching from spin 1 to spin $\frac{1}{2}$ would occur on the same temperature scale over which the correlations were building, so that any effects of that first quenching would be difficult to distinguish. And, of course, we are not actually in the $\mathcal{J}' \gg T_K$ regime. Nonetheless, our results for $T\chi^{(u)}$ and $\langle \sigma_{z1}\sigma_{z2} \rangle$ are consistent with a ferromagnetically correlated two-spin complex with reduced Kondo temperature(s). As predicted in Sec. II C for this case, $T\chi \sim \frac{1}{2}T\chi^{(u)}$, and $T\chi^{(s)}$ is much reduced from the single-impurity $T\chi$

C. $|\mathcal{J}| \gtrsim T_K$: Kondo Hamiltonian

We now consider two Kondo spins. We choose next-nearest-neighbor impurities on a one-dimensional hopping lattice, with the Hamiltonian of Eq. (25). As before, we set $t = \frac{1}{2}$ and $\mu_c = 0.0$, giving a band from -1 to 1 with $\rho = 0.32$ at the Fermi surface. We choose $J = 1.0$, so that $\rho J \approx 0.32$.

In Fig. 15, we show $\langle \sigma_{z1}\sigma_{z2} \rangle$ versus $\log_2(T)$, as well as the prediction of the RKKY effective Hamiltonian with RKKY $\mathcal{J}$ (open diamonds), with an arrow signifying the Kondo temperature. We thus see, as before, that $\langle \sigma_{z1}\sigma_{z2} \rangle$ develops roughly according to a RKKY effective Hamiltonian when $T \ll D$, though the correlations are slightly overestimated due to the lowest-order-

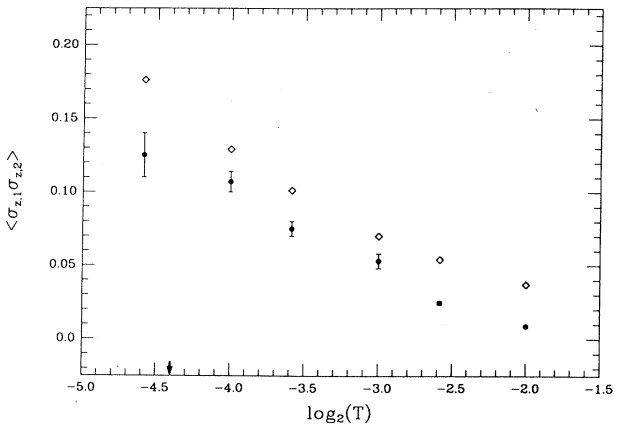

FIG. 15. $\langle\sigma_{z1}\sigma_{z2}\rangle$ vs $\log_2(T)$ for Kondo next-nearest neighbors on one-dimensional nearest-neighbor-hopping lattice, with $t=\frac{1}{2}$, $J=1.0$, and $\mu_c=0.0$. Solid circles, Monte Carlo data. Open diamonds, RKKY predictions. T_K shown by arrow.

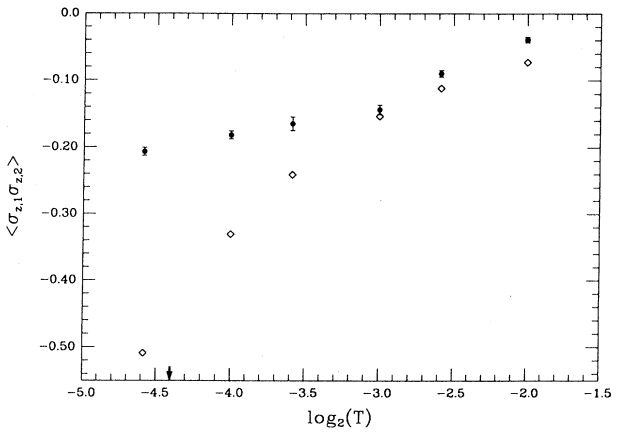

FIG. 17. $\langle\sigma_{z1}\sigma_{z2}\rangle$ vs $\log_2(T)$ for same parameters as Fig. 15, except that Kondo spins are nearest neighbors. Solid circles, Monte Carlo data. Open diamonds, RKKY predictions. T_K shown by arrow.

only calculation of $\mathcal{J}$. It appears that the correlations are beginning to quench at $\beta\approx 24$; calculated from Eq. (22), $T_K\sim\frac{1}{20}$.

In Fig. 16, we show from top to bottom $T\chi^{(u)}$, $T\chi$, and $T\chi^{(s)}$ for the two-impurity system, as well as $T\chi$ for a single impurity (open diamonds). As in the Anderson case, $T\chi^{(u)}$ is enhanced over $T\chi$, and both $T\chi^{(u)}$ and $T\chi$ are enhanced over the single-impurity $T\chi$. $T\chi^{(s)}$ is very slightly reduced, if at all, from the single-impurity $T\chi$. This is different from the more substantial reduction in the Anderson case; it is most likely due to the fact that $|\mathcal{J}'|/T_K\approx 1.5$ for the Anderson system, which is significantly larger than $|\mathcal{J}|/T_K\approx 0.6$ for the Kondo system. Thus, in the Kondo system here, we appear qualitatively closer to the $|\mathcal{J}|/T_K\ll 1$ limit of Sec. V A.

If, as before, we attempt to model the susceptibilities

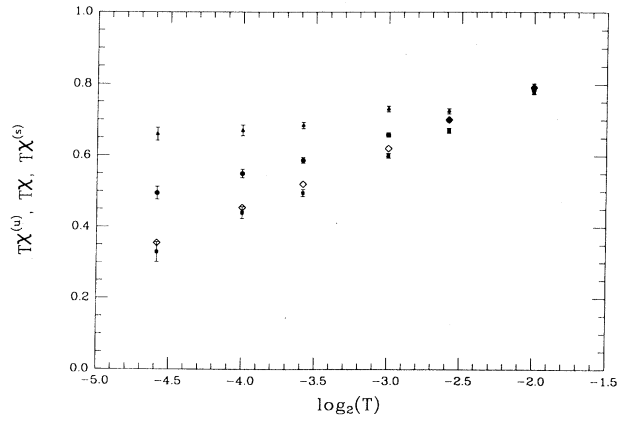

FIG. 16. From top to bottom, solid symbols, $T\chi^{(u)}$ (solid triangles), $T\chi$ (solid circles), and $T\chi^{(s)}$ (solid squares) vs $\log_2(T)$ for same parameters as Fig. 15. Open diamonds, $T\chi$ for a single impurity. Errors, if not shown, are less than or equal to symbol size.

using the $|\mathcal{J}|\gg T_K$ predictions of scaling theory,[3] we find that $T_K^{(1)}=T_K^{(2)}\approx 0.044$. The limit $|\mathcal{J}|\gg T_K$ is, of course, completely inapplicable here. Our results, rather, again clearly indicate the development of a ferromagnetically correlated complex with reduced uniform susceptibility Kondo temperature(s).

Lastly, we compare the properties of spin correlations for $|\mathcal{J}|/T_K\sim 1$ when $\mathcal{J}$ is ferromagnetic and when it is antiferromagnetic. To do this, we show in Fig. 17 antiferromagnetic spin correlations with the same parameter values as the ferromagnetic next-nearest-neighbor (NNN) correlations of Fig. 15 (i.e., the T_K's are the same). The saturation appears to occur at higher temperatures in the antiferromagnetic case. This may possibly be related to the enhanced on-site susceptibility for $\mathcal{J}$ ferromagnetic ("lower T_K") and to the similarly dehanced on-site susceptibility for antiferromagnetic $\mathcal{J}$ in this regime ("higher T_K"). As mentioned previously, the Kondo system corresponds to the $D\ll U$ limit of two Anderson impurities. However, we have not investigated whether this different saturation behavior occurs in the Anderson case when $D\gg U$.

VI. DEPENDENCE ON DISTANCE

We now consider the effect of interimpurity distance on the correlations between the two spins. Naively, we might expect the correlations to follow the same RKKY development independently of distance. However, we find that this is not the case.

In Fig. 18, we show $\langle\sigma_{z1}\sigma_{z2}\rangle$ versus $\log_2(T)$ for the same general parameters as Figs. 15 and 17; however, the impurities are now a distance of four lattice sites apart, as for Fig. 12. We also show with diamonds the correlation development predicted from the RKKY effective Hamiltonian. In contrast to Figs. 15 and 17, we see that the RKKY predictions grossly overestimate the actual spin correlations.

We can see this effect even more clearly in Fig. 19. Here, we set $t=\frac{1}{2}$, $J=1.2$ ($\rho J\approx 0.384$), and $\mu_c=0.0$, giving $T_K\approx 0.090$, and consider impurities a distance of

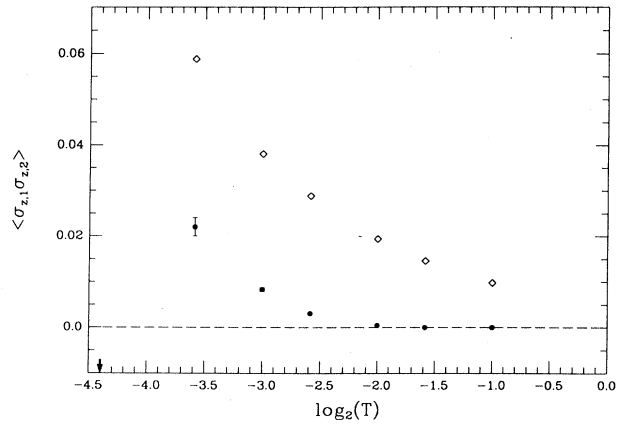

FIG. 18. $\langle\sigma_{z1}\sigma_{z2}\rangle$ vs $\log_2(T)$ for same parameters as Fig. 15, except that Kondo spins are a distance of four lattice sites apart. Solid circles, Monte Carlo data. Open diamonds, RKKY predictions. T_K shown by arrow.

eight lattice sites apart. We note that the reduction from RKKY predictions becomes greater as the distance between impurities increases.

We can explain this behavior qualitatively as follows. The RKKY interaction between the two impurity spins is mediated by the conduction electrons. As the temperature is lowered, the conduction-electron scattering (or correlation) length increases. When this length becomes of the order of the interimpurity distance, the two impurity spins begin to communicate, and spin correlation development will start to follow the RKKY predictions above the Kondo temperature. However, if the conduction scattering length is still less than the interimpurity distance at $T\sim T_K$, the spin correlations will be greatly reduced from those expected from a simple competition between Kondo and RKKY effects.

Thus, we see that conduction-electron correlation length, as well as RKKY and Kondo effects, can play a role in the development of Kondo impurity spin correlations. This general result may be relevant in particular to "dirty" systems.

VII. CROSSOVER BETWEEN SMALL AND LARGE COUPLING

We now consider the transition between the small-coupling regime ($\rho J<1$) previously considered and the large-coupling regime ($\rho J>1$). Though the latter regime is less physical, we include it here for completeness.

In Fig. 20, we show $\langle\sigma_{z1}\sigma_{z2}\rangle$ versus ρJ at $\beta=8$ and $\mu_c=0.0$ for two nearest-neighbor impurities, on the $t=\frac{1}{6}$ hopping lattice of Eq. (23). At first, the correlations increase as ρJ increases; for sufficiently small J, they will be proportional to $\beta\rho J^2$. However, as ρJ increases, we eventually enter the large-coupling regime, where perturbation in $1/\rho J$ rather than ρJ is valid. In this regime, it is favorable for the impurity spins to "trap" a single conduction electron at each impurity site to form a singlet state; the consequent lowering of the "magnetic" energy more than compensates for the increase in localization energy of the conduction electron. Thus, we are essentially doing a perturbation in $1/\rho J$ around an unperturbed state of two independent singlets; the perturbing term here is the conduction electron hopping. In this large-coupling limit, correlations are always antiferromagnetic for nearest neighbors.

In Fig. 21, we show $\langle\sigma_{z1}\sigma_{z2}\rangle$ versus $\log_2(T)$ for the same parameters as Fig. 20, except that $\mu_c=-0.5$. For small ρJ, this gives a ferromagnetic RKKY interaction; however, as ρJ increases, correlations again become antiferromagnetic as we enter the large-coupling regime. Thus, we see a crossover in the sign of the spin correlations as ρJ increases.

This crossover may be relevant to the shifting with U observed in Ref. 4 of the first node of spin correlations between two Anderson impurities. It was found that, as U decreases, the closest interimpurity distance at which

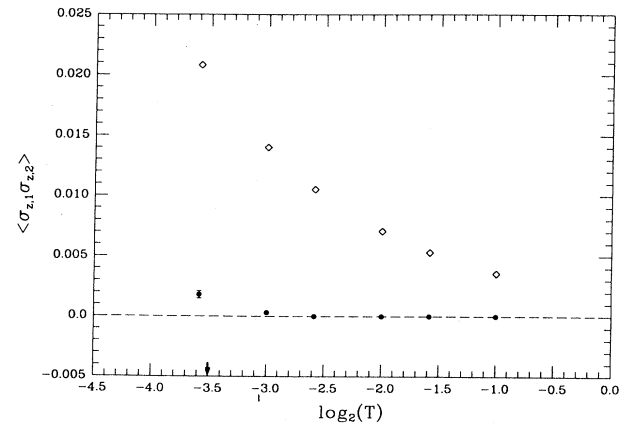

FIG. 19. $\langle\sigma_{z1}\sigma_{z2}\rangle$ vs $\log_2(T)$ for same parameters as Fig. 15, except that $J=1.2$ and Kondo spins are a distance of eight lattice sites apart. Solid circles, Monte Carlo data. Open diamonds, RKKY predictions. T_K shown by arrow.

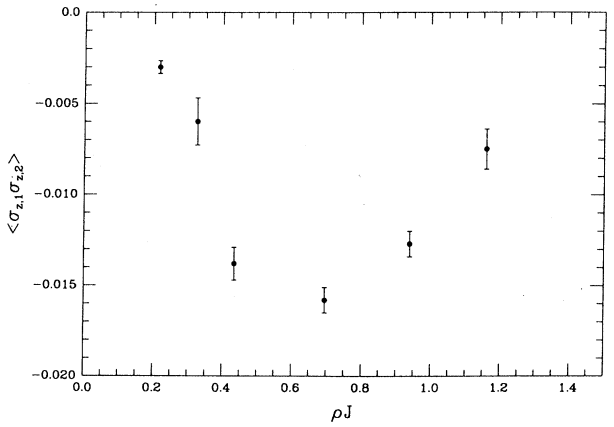

FIG. 20. $\langle\sigma_{z1}\sigma_{z2}\rangle$ vs ρJ for Kondo nearest-neighbor spins on three-dimensional nearest-neighbor-hopping lattice. $t=\frac{1}{6}$, $\mu_c=0.0$, and $\beta=8$.

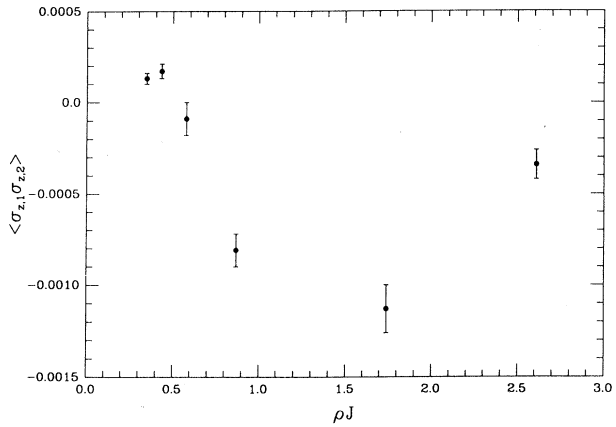

FIG. 21. Same as Fig. 14, but $\mu_c = -0.5$.

the spin correlations changed from ferromagnetic to antiferromagnetic became smaller when all other parameters were held constant. Decreasing U implies an increasing J (and, hence ρJ) from the Schrieffer-Wolff transformation.[14] Thus, this node shifting is consistent with the change from ferromagnetic to antiferromagnetic correlations with increasing ρJ just noted.

Lastly, in Fig. 22, we show $\langle \sigma_{z1}\sigma_{z2} \rangle$ for the same parameters as the two previous graphs, except that $\rho J \approx 1.70$ ($J=2.0$) and μ_c is varied (the band extends from -1 to 1). This illustrates the large-coupling perturbation picture; as long as the chemical potential lies within the conduction band, the two (here, nearest-neighbor) impurities will each trap a conduction electron to form two singlets, which will then be perturbed by the conduction-electron hopping. Thus, for large ρJ and μ_c inside the band, $\langle \sigma_{z1}\sigma_{z2} \rangle$ should be always antiferromagnetic and independent of μ_c, in agreement with results. This is very different from what would occur for small ρJ; in that case, $\langle \sigma_{z1}\sigma_{z2} \rangle$ would oscillate between antiferromagnetic and ferromagnetic values as μ_c (and, hence, k_F) was varied.

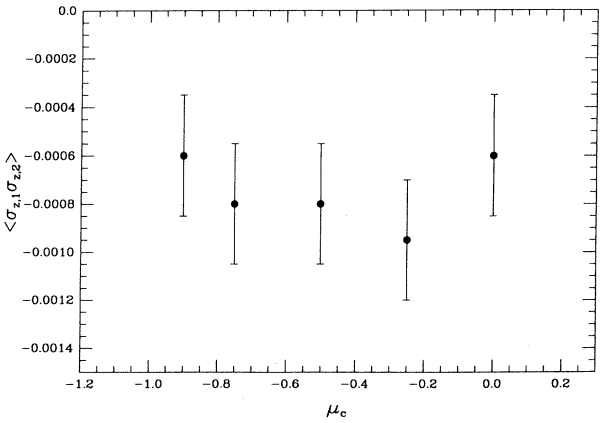

FIG. 22. $\langle \sigma_{z1}\sigma_{z2} \rangle$ vs μ_c for Kondo nearest-neighbor spins on three-dimensional nearest-neighbor-hopping lattice. $t=\frac{1}{6}$, $J=8, \beta=8$.

VIII. SUMMARY

Using an essentially exact quantum Monte Carlo algorithm, we investigated two interacting magnetic impurities in a metal for several different band structures. We focused on the two-impurity Kondo Hamiltonian, but also presented some new results for the two-impurity Anderson model. We were most interested in exploring the competition between RKKY interactions, with energy scale $\mathcal{J}$, which tend to "order" the two impurity spins into a triplet or singlet, and Kondo quenching effect, with energy scale

$$T_K \approx D(\rho J)^{1/2} e^{-1/\rho J} , \tag{27}$$

where D is the effective bandwidth, ρ is the density of states at the Fermi level, and J is the Kondo coupling constant.

We considered first the case of antiferromagnetic RKKY interaction between the two impurities. For $\mathcal{J}/T_K$ small, where $\mathcal{J}$ is the RKKY coupling constant, we found that correlations developed following a RKKY effective Hamiltonian $H_{\text{eff}} = \mathcal{J}\mathbf{S}_1 \cdot \mathbf{S}_2$ down to approximately the Kondo temperature, where they leveled off and saturated. We then investigated values of $\mathcal{J}/T_K$ and the corresponding ρJ's close to those where an anomalous staggered susceptibility and coefficient of specific heat γ were predicted from renormalization-group work.[5] Correlations again followed a RKKY effective Hamiltonian and then quenched at around T_K; more importantly, nothing unusual was seen in the staggered susceptibility. Whether this might be due to a different staggered susceptibility definition, a different band structure, or an approximation in the renormalization-group work[7] is not clear. Another possibility which should be mentioned is finite temperature effects, but our data strongly suggest that this is not the case. Recent auxiliary boson mean-field work,[6] however, was not inconsistent with our results. For all values of antiferromagnetic $\mathcal{J}/T_K$ investigated, correlations, staggered susceptibility, on-site susceptibility, and uniform susceptibility were qualitatively and sometimes quantitatively understandable in terms of the expected parametrizations of Sec. III.

Second, we considered the case of ferromagnetic RKKY interactions for both Kondo and Anderson models. As before, we found that spin correlation development followed a RKKY effective Hamiltonian down to approximately the Kondo temperature, where quenching would then occur. For $|\mathcal{J}|/T_K \ll 1$, we found that both the low-temperature on-site susceptibility [Eq. (4)] and the uniform susceptibility were enhanced over the single-impurity susceptibility, parametrizable by a decreased Kondo temperature. This was in contrast to the antiferromagnetic $\mathcal{J}/T_K \ll 1$ case, where the on-site susceptibility showed negligible change. Further enhancement of both on-site and uniform susceptibilities occurred for ferromagnetic $|\mathcal{J}|/T_K \gtrsim 1$. This suggests a ferromagnetically correlated complex with reduced Kondo temperature(s), possibly along the lines of scaling theory predictions[3] for $\mathcal{J} \gg T_K$. However, we did not specifically simulate the $\mathcal{J} \gg T_K$ regime.

Next, we considered the effect of interimpurity dis-

tance on the development of impurity spin correlations. We found that, in contrast to nearby impurities, impurities far away showed spin correlation development greatly reduced from the RKKY expectations. We explained this by noting that if the conduction-electron correlation length was less than the interimpurity distance at the Kondo temperature, the impurities would not have had a chance to "communicate" with each other before the spins were individually Kondo quenched. Thus, conduction electron correlation length as well as Kondo temperature and RKKY interactions can play a role in the development of spin correlations.

Lastly, we investigated the crossover from small ($\rho J \ll 1$) into large ($\rho J \gg 1$) coupling. We found that in the large-coupling limit, one conduction electron would be "trapped" at each impurity spin site in a singlet, with perturbation being the conduction-electron hopping, if the Fermi level was inside the conduction band. Thus, in contrast to the small-coupling regime, nearest-neighbor spin correlations were always antiferromagnetic and independent of chemical potential, and decreased with ρJ at all temperatures. As one consequence of this, for example, correlations which were initially ferromagnetic for small ρJ would eventually become antiferromagnetic as ρJ increased. This finding provides a qualitative explanation for the shift in the nodes of the spin correlations found in Ref. 4 as U was changed.

If one attempts to apply our results to heavy-fermion systems, certain effects are of course missed; for example, spin-glass effects for random impurities, and coherence effects and the possibility of instabilities in narrow renormalized bands for the lattice case. However, we expect the general picture of RKKY interactions versus Kondo quenching to remain valid, as indicated by recent Anderson lattice work.[19] Within this picture, if the lattice Kondo temperature is higher than the transition temperature of the corresponding RKKY spin lattice, there will be no long-range order, though significant short-range "precursor" order may develop. If the lattice Kondo temperature is lower than the RKKY spin lattice transition temperature, however, long-range order will occur. The effective moments may be reduced, though, as the Kondo effect prevents further spin correlation development below the Kondo temperature.

ACKNOWLEDGMENTS

One of us (R.M.F.) would like to thank B. A. Jones and A. J. Millis for very interesting and helpful conversations. This work was supported by National Science Foundation (NSF) Grant No. DMR 85-17756 as well as contributions from AT&T Bell Laboratories. The calculations were done on the Cray at the San Diego Supercomputer Center.

APPENDIX A: PROCEDURE FOR SIMULATION OF TWO-IMPURITY KONDO MODEL

We begin with the Kondo two-impurity Hamiltonian

$$H' = H_0 + H_I' \ , \tag{A1}$$

where

$$H_0 = \sum_{\mathbf{k},\sigma} \epsilon_{\mathbf{k}} c^{\dagger}_{\mathbf{k}\sigma} c_{\mathbf{k}\sigma} \tag{A2}$$

and

$$H_I' = J[\mathbf{S}_c(\mathbf{R}_1)\cdot\mathbf{S}_1 + \mathbf{S}_c(\mathbf{R}_2)\cdot\mathbf{S}_2] \ . \tag{A3}$$

Here,

$$\mathbf{S}_c(\mathbf{R}_m) = \sum_{\sigma,\sigma'} c^{\dagger}_{m\sigma} \left[\frac{1}{2} \boldsymbol{\sigma}_{\sigma\sigma'} \right] c_{m\sigma'} \tag{A4}$$

is the normalized conduction electron spin at site $\mathbf{R}_m$, with

$$c_{m\sigma} = \frac{1}{\sqrt{N}} \sum_{\mathbf{k}} e^{i\mathbf{k}\cdot\mathbf{R}_m} c_{\mathbf{k}\sigma} \ . \tag{A5}$$

N is the number of $\mathbf{k}$ vectors, $\boldsymbol{\sigma}_{\sigma\sigma'}$ denotes the Pauli matrices, and the $\mathbf{S}_m$'s refer to the two impurity spins.

Because we are utilizing a fermion algorithm, however, we will not use the Hamiltonian of Eqs. (A1)–(A5) directly. Rather, we will simulate the Hamiltonian $H = H_0 + H_I$ with interaction term

$$H_I = J[\mathbf{S}_c(\mathbf{R}_1)\cdot\mathbf{S}_{f1} + \mathbf{S}_c(\mathbf{R}_2)\cdot\mathbf{S}_{f2}] \ , \tag{A6}$$

where

$$\mathbf{S}_{fm} = \sum_{\sigma,\sigma'} f^{\dagger}_{m\sigma} (\tfrac{1}{2}\boldsymbol{\sigma}_{\sigma\sigma'}) f_{m\sigma'} \ , \tag{A7}$$

and the $f_{m\sigma}$'s refer to impurity electron states. However, during the simulation we will apply a projection operator P which projects onto only singly occupied f states at each impurity site, to convert the f electrons into "spins." Because H itself commutes with the total number of f electrons at each impurity site, it cannot propagate singly occupied f states into zero or doubly occupied f states. Thus, for a given operator O which conserves the number of f electrons at each impurity site,

$$\frac{\mathrm{Tr}(Pe^{-\beta H}O)}{\mathrm{Tr}(Pe^{-\beta H})} = \frac{\mathrm{Tr}(e^{-\beta H'}O)}{\mathrm{Tr}(e^{-\beta H'})} \ , \tag{A8}$$

with an analogous result holding for susceptibilities. All operators and susceptibilities which we consider have this conservation property. Thus, our procedure is completely equivalent to simulating the desired Hamiltonian of Eqs. (A1)–(A5).

The form of P which we choose is

$$P = \prod_{m=1}^{2} \exp\{(-U_P)[\tfrac{1}{4} + (n_{fm\uparrow} - \tfrac{1}{2})(n_{fm\downarrow} - \tfrac{1}{2})]\} \ . \tag{A9}$$

In our simulations, we always use $U_P \geq 12$; this gives a local moment $\langle (n_{fm\uparrow} - n_{fm\downarrow})^2 \rangle$ which differs from 1 by no more than a few parts in a thousand.

We now write the interaction term H_I first as

$$H_I = H_I^{(1)} + H_I^{(2)} \ , \tag{A10}$$

where

$$H_I^{(m)} = J\mathbf{S}_c(\mathbf{R}_m)\cdot\mathbf{S}_{fm} \ . \tag{A11}$$

Next, we write out each $H_I^{(m)}$ as

$$H_I^{(m)}=H_1^{(m)}+H_2^{(m)}+H_3^{(m)} , \tag{A12}$$

where

$$H_1^{(m)}=\frac{J}{2}c_{m\uparrow}^{\dagger}c_{m\downarrow}f_{m\downarrow}^{\dagger}f_{m\uparrow} , \tag{A13}$$

$$H_2^{(m)}=\frac{J}{2}c_{m\downarrow}^{\dagger}c_{m\uparrow}f_{m\uparrow}^{\dagger}f_{m\downarrow} , \tag{A14}$$

and

$$H_3^{(m)}=\frac{J}{4}(n_{cm\uparrow}-n_{cm\downarrow})(n_{fm\uparrow}-n_{fm\downarrow}) . \tag{A15}$$

We then approximate the partition function by using the Trotter approximation,[20]

$$Z=\mathrm{Tr}(Pe^{-\beta H}) \tag{A16}$$

$$=\mathrm{Tr}[P(e^{-(\Delta\tau)H})^L] , \tag{A17}$$

where $\Delta\tau=\beta/L$,

$$\approx\mathrm{Tr}\left\{P\left[e^{-(\Delta\tau)H_0}\left[\prod_m e^{-(\Delta\tau)H_1^{(m)}}e^{-(\Delta\tau)H_2^{(m)}}\times e^{-(\Delta\tau)H_3^{(m)}}\right]\right]^L\right\} . \tag{A18}$$

$H_1^{(m)}$ and $H_2^{(m)}$ are not Hermitian, so that one might expect the Trotter error in observables[11] and susceptibilities[12] to be of order $\Delta\tau$ rather than $(\Delta\tau)^2$. However, we show in Appendix B that the error linear in $\Delta\tau$ again vanishes for the quantities of interest due to invariance of the Hamiltonian under spin label exchange. Thus, we can extrapolate in $(\Delta\tau)^2$ as usual.

We now decouple the interaction terms into bilinear fermion terms using generalized discrete Hubbard-Stratonovitch transformations.[13] For P, we use

$$\exp\{(-U_P)[\tfrac{1}{4}+(n_{fm\uparrow}-\tfrac{1}{2})(n_{fm\downarrow}-\tfrac{1}{2})]\}$$
$$=\tfrac{1}{2}\exp\left[-\frac{U_p}{2}\right]\mathrm{Tr}_\sigma\exp[\lambda_P\sigma(n_{fm\uparrow}-n_{fm\downarrow})] , \tag{A19}$$

where $\cosh\lambda_P=e^{U_P/2}$ and σ takes the values ±1. For $e^{-(\Delta\tau)H_1^{(m)}}$, we use

$$\exp\left[-\frac{J(\Delta\tau)}{2}(c_{m\uparrow}^{\dagger}c_{m\downarrow}f_{m\downarrow}^{\dagger}f_{m\uparrow}\right]$$
$$=\tfrac{1}{2}\mathrm{Tr}_\sigma\exp[\lambda_1\sigma(c_{m\uparrow}^{\dagger}f_{m\uparrow}+f_{m\downarrow}^{\dagger}c_{m\downarrow})] , \tag{A20}$$

where $\lambda_1=(J(\Delta\tau)/2)^{1/2}$, with an analogous decoupling for $e^{-(\Delta\tau)H_2^{(m)}}$,

$$\exp\left[-\frac{J(\Delta\tau)}{2}(c_{m\downarrow}^{\dagger}c_{m\uparrow}f_{m\uparrow}^{\dagger}f_{m\downarrow})\right]$$
$$=\tfrac{1}{2}\mathrm{Tr}_\sigma\exp[\lambda_1\sigma(c_{m\downarrow}^{\dagger}f_{m\downarrow}+f_{m\uparrow}^{\dagger}c_{m\uparrow})] . \tag{A21}$$

We could also group the bilinear terms in Eqs. (A20)–(A21) by particle type (c or f) rather than spin. However, we find that grouping the terms by spin leads to a much smaller percentage of negative determinants in our simulation. The reason is that the determinants for spin up and spin down have very similar form, so that when one changes sign the other one frequently does also. For example, if we retain only the spin-flip terms of the Hamiltonian (the $H_1^{(m)}$'s and $H_2^{(m)}$'s), as well as H_0, a particle-hole transformation shows that the net determinant is always positive in the symmetric case, in analogy to the results for a symmetric Hubbard[13] or Anderson[10] model; the same holds true if we retain only the $H_3^{(m)}$'s with H_0. Also, we find that grouping the terms by spin gives less statistical error even when there are almost no negative determinants.

Lastly, for $e^{-(\Delta\tau)H_3^{(m)}}$, we utilize the fact that, because of P, the operators $n_{fm\uparrow}-n_{fm\downarrow}$ can only take on the values ±1. Thus, we can effectively write

$$\exp\left[-\frac{J(\Delta\tau)}{4}(n_{cm\uparrow}-n_{cm\downarrow})(n_{fm\uparrow}-n_{fm\downarrow})\right]$$
$$=\exp\left[-\frac{J(\Delta\tau)}{4}n_{cm\uparrow}\sigma_{mz}\right]\exp\left[\frac{J(\Delta\tau)}{4}n_{cm\downarrow}\sigma_{mz}\right] . \tag{A22}$$

Then,

$$\exp\left[-\frac{J(\Delta\tau)}{4}n_{cm\uparrow}\sigma_{mz}\right]=\left[\exp\left[-\frac{J(\Delta\tau)}{4}[\tfrac{1}{2}(\sigma_{mz}+1)]\right]\right]\tfrac{1}{2}\mathrm{Tr}_\sigma\exp\{\lambda_2\sigma[n_{cm\uparrow}-\tfrac{1}{2}(\sigma_{mz}+1)]\} , \tag{A23}$$

where $\cosh\lambda_2=e^{J(\Delta\tau)/4}$, and

$$e^{[J(\Delta\tau)/4]n_{cm\downarrow}\sigma_{mz}}=(e^{[J(\Delta\tau)/4][(1/2)(\sigma_{mz}-1)]})\times\tfrac{1}{2}\mathrm{Tr}_\sigma e^{\lambda_2\sigma[n_{cm\downarrow}+(1/2),\sigma_{mz}-1)]} . \tag{A24}$$

Converting back to fermion notation, we obtain the form

$$e^{-(\Delta\tau)H_3^{(m)}}=e^{-J(\Delta\tau)/4}(\tfrac{1}{4})\mathrm{Tr}_{\sigma\sigma'}\times(e^{-(\lambda_2/2)(\sigma+\sigma')}e^{\lambda_2\sigma n_{cm\uparrow}}e^{\lambda_2\sigma' n_{cm\downarrow}}\times e^{-(\lambda_2/2)(\sigma-\sigma')n_{f\uparrow}}e^{(\lambda_2/2)(\sigma-\sigma')n_{f\downarrow}}) . \tag{A25}$$

Thus, after isolating the interaction term and splitting it up using the Trotter approximation, we have decoupled the term by introducing four Ising fields. This decoupling will occur at each impurity site $m=1$, 2, and "imaginary time" slice $l=1,\ldots,L$.

We note that it is also possible to decouple the interaction term itself with no Trotter error. To do this, we first write

$$e^{-(\Delta\tau)H_I}=e^{-(\Delta\tau)H_I^{(1)}}e^{-(\Delta\tau)H_I^{(2)}}, \tag{A26}$$

since

$$[H_I^{(1)},H_I^{(2)}]=0 . \tag{A27}$$

Then,

$$e^{-(\Delta\tau)H_I^{(m)}}=e^{-(\Delta\tau)(H_1^{(m)}+H_2^{(m)})}e^{-(\Delta\tau)H_3^{(m)}}, \tag{A28}$$

since

$$[H_1^{(m)}+H_2^{(m)},H_3^{(m)}]=0 . \tag{A29}$$

Next, we use the identity for $H_1^{(m)}$ and $H_2^{(m)}$,

$$e^{-(\Delta\tau)(H_1^{(m)}+H_2^{(m)})}=\tfrac{1}{2}\mathrm{Tr}_n(e^{-\alpha_1 nH_1^{(m)}}e^{[-\alpha_1(1-n)-\alpha_2 n]H_2^{(m)}}\times e^{-\alpha_2(1-n)H_1^{(m)}}) , \tag{A30}$$

where

$$\alpha_1=\left[\frac{2}{J}\right](e^{J(\Delta\tau)/2}-1) , \tag{A31}$$

$$\alpha_2=\left[\frac{2}{J}\right](1-e^{-J(\Delta\tau)/2}) , \tag{A32}$$

and n here takes on the values 0 and 1. Finally, the remaining interaction terms in Eq. (A30) are decoupled as before; however, there are now six rather than four two-valued fields at each impurity site and imaginary time slice.

This latter procedure restores rotational symmetry for finite $\Delta\tau$, broken in the breakup of Eq. (A18), and does not seem to qualitatively worsen statistics. However, surprisingly, it does not appear to significantly decrease the net Trotter error in most parameter regimes. We have found that it may even increase the error in some cases due to apparently fortuitous cancellations in the nonsymmetric breakup. Further, the breakup of Eq. (A18) gives us two different values of spin quantities for finite $\Delta\tau$, measured in the x and z directions. If both quantities are seen to approach the same value as $(\Delta\tau)^2\to 0$, our confidence in the extrapolation is increased; in many cases, one quantity approaches from above and one from below. Therefore, for our simulations, we have primarily used the decoupling procedure of Eqs. (A18)–(A24).

Thus, our approximate partition function becomes

$$\begin{aligned}Z_{\mathrm{approx}}=\kappa\,\mathrm{Tr}_{\{\sigma\}}&\left[\left[\prod_{l=1}^{L}\left[\prod_{m=1}^{2}e^{-(\lambda_2/2)(\sigma_{2lm}+\sigma_{4lm})}\right]\right]\right.\\
&\times\left\{\mathrm{Tr}_{\{n\uparrow\}}\left[\prod_{l=1}^{L}e^{-(\Delta\tau)H_0(\uparrow)}\left[\prod_{m=1}^{2}e^{\lambda_1\sigma_{1lm}c_{m\uparrow}^{\dagger}f_{m\uparrow}}e^{\lambda_1\sigma_{2lm}f_{m\uparrow}^{\dagger}c_{m\uparrow}}e^{\lambda_2\sigma_{3lm}n_{cm\uparrow}}e^{-(\lambda_2/2)(\sigma_{3lm}-\sigma_{4lm})n_{fm\uparrow}}\right]\right]\right.\\
&\left.\times\left[\prod_{m=1}^{2}e^{\lambda_p\sigma_{pm}n_{fm\uparrow}}\right]\right\}\left\{\mathrm{Tr}_{\{n\downarrow\}}\left[\prod_{l=1}^{L}e^{-(\Delta\tau)H_0(\downarrow)}\left[\prod_{m-1}^{2}e^{\lambda_1\sigma_{1lm}f_{m\downarrow}^{\dagger}c_{m\downarrow}}e^{\lambda_1\sigma_{2lm}c_{m\downarrow}^{\dagger}f_{m\downarrow}}\right.\right.\right.\\
&\left.\left.\left.\times e^{\lambda_2\sigma_{4lm}n_{cm\downarrow}}e^{(\lambda_2/2)(\sigma_{3lm}-\sigma_{4lm})n_{fm\downarrow}}\right]\right]\right.\\
&\left.\left.\times\left[\prod_{m=1}^{2}e^{-\lambda_p\sigma_{pm}n_{fm\downarrow}}\right]\right\}\right] ,\end{aligned} \tag{A33}$$

where we used the cyclic property of the trace to shift the position of P. Here, κ is some constant which cancels out when we take expectation values; σ_{nlm} refers to the nth Ising spin at site m and imaginary time slice l (the σ_{pm}'s are the projector spins); $\mathrm{Tr}_{\{\sigma\}}$ refers to the trace over the Ising field; $\mathrm{Tr}_{\{n\uparrow\}}$ and $\mathrm{Tr}_{\{n\downarrow\}}$ refer to traces over the up and down fermions, respectively; and $H_0(\uparrow)$ and $H_0(\downarrow)$ refer to the spin-up and spin-down parts of H_0. In essence, we have reduced the partition function to bilinear form in the fermion operators, separating the traces over spin-up and -down orbitals, at the expense of introducing an Ising field.

Taking the trace over the fermions then yields[9,21]

$$Z_{\mathrm{approx}}=\mathrm{Tr}_{\{\sigma\}}\left[e^{\mathcal{S}\{\sigma\}}\left[\prod_{S=\pm 1}^{N,L}\det O_S\{\sigma\}\right]\right] , \tag{A34}$$

where O_S is an $NL\times NL$ matrix, with N here the number of spatial sites (or $\mathbf{k}$ vectors) for the conduction electrons plus two for the impurity orbitals. $e^{\mathcal{S}\{\sigma\}}$ refers to the pure Ising part of Eq. (A33). Thus, we have an effective "Boltzmann weight" for each Ising configuration.

Written out in the imaginary time direction, the matrix O_S is formally

$$O_S=\begin{bmatrix} I & 0 & \cdots & e^{-(\Delta\tau)K}e^{V_L^S}e^{V_P^S} \\ -e^{-(\Delta\tau)K}e^{V_1^S} & I & & 0 \\ 0 & -e^{-(\Delta\tau)K}e^{V_2^S} & & \vdots \\ 0 & 0 & \ddots & \vdots \\ \vdots & \vdots & & I \end{bmatrix} . \tag{A35}$$

Here, K is an $N\times N$ matrix given by

$$H_0=\sum_{i,j,\sigma} a_{i\sigma}^{\dagger}K_{ij}a_{j\sigma} , \tag{A36}$$

where the $a_{i\sigma}$'s refer to conduction or impurity states, with i and j running over all orbital degrees of freedom. V_P^S is a potential acting only at each impurity orbital,

$$V_P^S=\sum_{m=1}^{2} |fms\rangle S\lambda_p\sigma_{pm}\langle fms| , \tag{A37}$$

so that $e^{V_P^S}$ is diagonal, with only two diagonal entries not equal to one. The V_l^S's, for $l=1,\ldots,L$, are formally potentials which act only at the impurity sites, but which couple the conduction electron orbitals localized at each site with the impurity orbital. Thus, they can be visualized as 2×2 potentials. Considering the spin up electrons, for example, one obtains from Eq. (A33)

$$\langle fms|e^{V_l^S}|fm's\rangle=[1+\lambda_1^2\sigma_{1lm}\sigma_{2lm}] \times e^{-(\lambda_2/2)(\sigma_{3lm}-\sigma_{4lm})}\delta_{mm'} , \tag{A38}$$

$$\langle fms|e^{V_l^S}|cm's\rangle=\lambda_1\sigma_{2lm}e^{-(\lambda_2/2)(\sigma_{3lm}-\sigma_{4lm})}\delta_{mm'} , \tag{A39}$$

$$\langle cms|e^{V_l^S}|fm's\rangle=\lambda_1\sigma_{1lm}e^{\lambda_2\sigma_{3lm}}\delta_{mm'} , \tag{A40}$$

and

$$\langle cms|e^{V_l^S}|cm's\rangle=e^{\lambda_2\sigma_{3lm}}\delta_{mm'} . \tag{A41}$$

Otherwise,

$$\langle ai,s|e^{V_l^S}|aj,s\rangle=\delta_{ij} . \tag{A42}$$

For a given Ising configuration, the Green's function matrix g_S is given by the inverse of O_S,

$$g_S=O_S^{-1} . \tag{A43}$$

Given two arbitrary Ising configurations with potentials V and V' where, corresponding to Eq. (A35),

$$e^{V}=\begin{bmatrix} e^{V_1} & 0 & 0 \\ 0 & e^{V_2} & \\ \vdots & & \\ \vdots & & e^{V_L}e^{V_P} \end{bmatrix} \tag{A44}$$

(we drop the spin index S here for simplicity), we find that the Green's function matrix obeys the Dyson-type equation[9]

$$g'=g+(g-I)(e^{-V}e^{V'}-I)g' . \tag{A45}$$

Further, because of the local nature of the potentials, we have

$$g'_{MM}=g_{MM}+(g_{MM}-I)(e^{-V}e^{V'}-I)g'_{MM} , \tag{A46}$$

where g_{MM} is now a $4L\times 4L$ matrix, corresponding to the two-impurity sites, each with an associated impurity and conduction orbital, and the L time slices. In essence, therefore, if we are concerned with impurity properties, we need only consider the impurity-site part of g, g_{MM}.

To begin the simulation, then, we set all interactions equal to zero. The matrix g_{MM} is then given by the noninteracting Green's function matrix g^0_{MM}; this is easily calculated even for an essentially infinite system, and is the only point at which system size enters into our computation. We next turn on the Ising field (for example, randomly), giving a potential V, and obtain the starting g_{MM} from Eq. (A46) by inverting a $4L\times 4L$ matrix,

$$g_{MM}=[I-(g^0_{MM}-I)(e^{V}-I)]^{-1}g^0_{MM} . \tag{A47}$$

We then proceed by sequentially proposing changes in the Ising field configurations. Assume that we attempt a change at site m and imaginary time slice l. Then, as in the related lattice algorithm,[21] the ratio of determinants between the old and new configurations is given by

$$R_S=\frac{\det[O_S\{\sigma'\}]}{\det[O_S\{\sigma\}]} \tag{A48}$$

$$=\det\{I+[I-g^S_{MM}(l,l)](e^{-V^S_{lm}}e^{(V^S_{lm})'}-I)\} . \tag{A49}$$

On the right-hand side of Eq. (A49), the determinant is now that of a 2×2 matrix.

Let

$$R_0=e^{[\mathcal{S}\{\sigma'\}-\mathcal{S}\{\sigma\}]} , \tag{A50}$$

from Eq. (A34). Then, $R=R_0R_{\uparrow}R_{\downarrow}$ will be the ratio of the effective Boltzmann weights of the two Ising configurations. If $R/(R+1)$ is greater than a randomly selected number between 0 and 1, we accept the configuration change; otherwise, it is rejected. (If R is negative, we use the related sampling procedure at the end of Ref. 21.)

If the configuration change is accepted, we update g_{MM} using the relation[9]

$$g'_{m_1m_2}(l_1,l_2)=g_{m_1m_2}(l_1,l_2)+[g_{m_1m}(l_1,l)-\delta_{m_1m}\delta_{l_1l}]\times t_m(l)g_{mm_2}(l,l_2)\ , \tag{A51}$$

where

$$t_m(l)=(e^{-V_{lm}}e^{V'_{lm}}-I)\times\{I+[I-g_{mm}(l,l)][e^{-V_{lm}}e^{V'_{lm}}-I]\}^{-1}\ . \tag{A52}$$

As in Eq. (A49), all quantities in Eq. (A51) and Eq. (A52) are 2×2 matrices. This updating is the most time-consuming part of the computation; one sweep through the Ising field requires an amount of time proportional to $(4L)^3$.

One difference in this procedure between the present and other simulations is that we do not attempt to flip each Ising spin separately as we move through the Ising field configuration space. There are here 16 possible configurations of the four Ising spins at each impurity site and imaginary time slice, and it takes no more time to change several of these spins simultaneously than to change just one. Thus, we number the 16 possible configurations, generate a random integer from 1 to 16 (not including the current configuration number), and then decide whether or not to accept the new configuration corresponding to the generated number. We find that this speeds the walk through the Ising space, reducing correlation time and allowing for shorter runs.

Because of the bilinear form of Eq. (A33), Wick's theorem holds, and we can calculate correlation functions in the usual way.[13] For example, for the spin correlation between the two impurities, we measure

$$\langle\sigma_{1z}\sigma_{2z}\rangle=\langle(n_{f1\uparrow}-n_{f1\downarrow})(n_{f2\uparrow}-n_{f2\downarrow})\rangle \tag{A53}$$

in the z direction and

$$\langle\sigma_{1x}\sigma_{2x}\rangle=\langle(f^\dagger_{1\uparrow}f_{1\downarrow}+f^\dagger_{1\downarrow}f_{1\uparrow})(f^\dagger_{2\uparrow}f_{2\downarrow}+f^\dagger_{2\downarrow}f_{2\uparrow})\rangle \tag{A54}$$

in the x direction. Further, by approximating an integral by a sum, we can calculate susceptibilities. For the on-site spin susceptibility, for example, we measure using Simpson's rule

$$\chi_z=\frac{(\Delta\tau)}{3}\sum_{l=0}^{L-1}[3-(-1)^l]\langle[n_{f1\uparrow}(\tau_l)-n_{f1\downarrow}(\tau_l)]\cdot[n_{f1\uparrow}-n_{f1\downarrow}]\rangle\ , \tag{A55}$$

where $\tau_l=l(\Delta\tau)$, and

$$\chi_x=\frac{(\Delta\tau)}{3}\sum_{l=0}^{L-1}[3-(-1)^l]\langle[f^\dagger_{1\uparrow}(\tau_l)f_{1\downarrow}(\tau_l)-f^\dagger_{1\downarrow}(\tau_l)f_{1\uparrow}(\tau_l)]\cdot[f^\dagger_{1\uparrow}f_{1\downarrow}+f^\dagger_{1\downarrow}f_{1\uparrow}]\rangle\ . \tag{A56}$$

In summary, then, we begin with a fermion partition function and introduce a projector field to turn the impurity fermions into spins. We next use the Trotter approximation to isolate the interaction parts of the Hamiltonian. These interaction terms are then decoupled using discrete Hubbard-Stratonovitch transformations, leaving the partition function in bilinear form in a fluctuating Ising field. We consequently perform a Monte Carlo simulation on the Ising field, taking the trace over the fermions at each step of the process. Wick's theorem holds, due to the bilinear form of the decoupled partition function, and we can thus measure correlations and susceptibilities of interest.

APPENDIX B: VANISHING OF FIRST-ORDER TROTTER ERROR

We begin by considering a general density matrix operator

$$e^{-\beta H}=(e^{-(\Delta\tau)H})^L\ , \tag{B1}$$

where $\Delta\tau=\beta/L$. Using the Trotter approximation,[20] we then write

$$e^{-\beta H}\approx\left[\prod_{n=1}^{N}e^{-(\Delta\tau)H_n}\right]^L\ , \tag{B2}$$

where

$$H=\sum_{n=1}^{N}H_n\ , \tag{B3}$$

to obtain an approximate density matrix operator.

We now consider the error when this approximate density matrix operator is used to calculate the expectation value of a Hermitian operator O. From Ref. 11, this error is

$$\langle O\rangle_{\text{approx}}-\langle O\rangle=(\Delta\tau)[\langle D(\beta)O\rangle-\langle D(\beta)\rangle\langle O\rangle]+\text{order}(\Delta\tau)^2\ , \tag{B4}$$

where expectation values with no subscripts are those taken with the exact density matrix operator. Here,

$$D(\beta)=\int_0^\beta d\tau\,C(\tau) \tag{B5}$$

and

$$C=\tfrac{1}{2}\sum_{n=1}^{N}\sum_{n'<n}[H_{n'},H_n]\ . \tag{B6}$$

For the breakup of Eq. (A18), we find that

$$C=\tfrac{1}{2}[H_0,H_I]+\tfrac{1}{2}\sum_{m=1}^{2}[H_1^{(m)},H_2^{(m)}]\ , \tag{B7}$$

since

$$[H_I^{(1)},H_I^{(2)}]=0 \tag{B8}$$

and

$$[H_1^{(m)}+H_2^{(m)},H_3^{(m)}]=0 . \tag{B9}$$

H_0 and H_I are both Hermitian operators and thus, again from Ref. 11, the first commutator in Eq. (B7) will make no contribution to the error linear in $\Delta\tau$ for $\langle O\rangle_{\text{approx}}$, since it is anti-Hermitian. Therefore, we need only consider the second term, with non-Hermitian $H_1^{(m)}$ and $H_2^{(m)}$.

Now, $H_1^{(m)}$ and $H_2^{(m)}$ transform into each other if up and down spin labels are interchanged. Thus, the commutator $[H_1^{(m)},H_2^{(m)}]$ changes sign under the interchange of up and down spin labels.

The Hamiltonian H, however, is invariant under this spin label exchange. We thus have, simply renaming the "dummy" summed-over spin indices,

$$\langle D(\beta)\rangle=\beta\langle C\rangle \tag{B10}$$

$$=\left[\frac{\beta}{Z}\right]\mathrm{Tr}\left[e^{-\beta H}\sum_{m=1}^{2}[H_1^{(m)},H_2^{(m)}]\right] \tag{B11}$$

$$=\left[\frac{\beta}{Z}\right]\mathrm{Tr}\left[e^{-\beta H}\sum_{m=1}^{2}[H_2^{(m)},H_1^{(m)}]\right] , \tag{B12}$$

so that $\langle D(\beta)\rangle=0$. Identical reasoning holds for $\langle D(\beta)O\rangle$ if O is invariant under the interchange of up and down spin labels. This will include, for example, all spin and charge correlation operators. Thus, for all operators of interest, the error linear in $\Delta\tau$ vanishes, leaving a leading error of order $(\Delta\tau)^2$.

We now consider the case of an approximate susceptibility

$$\chi_{O,\text{approx}}=\left[\frac{\Delta\tau}{3}\right]\sum_{l=0}^{L-1}[3-(-1)^l]\langle O(\tau_l)O\rangle_{\text{approx}} -\beta\langle O\rangle_{\text{approx}}^2 , \tag{B13}$$

where $\tau_l=l\Delta\tau$, when compared to an exact susceptibility

$$\chi_O=\int_0^\beta d\tau\langle O(\tau)O\rangle-\beta\langle O\rangle^2 . \tag{B14}$$

If O is a spin, we set $\langle O\rangle_{\text{approx}}$ to zero by symmetry. If O refers to charge, the error in $\langle O\rangle_{\text{approx}}$ will be of order $(\Delta\tau)^2$. The replacement of an integral by a sum in Eq. (B13), using Simpson's rule, gives an error of order $(\Delta\tau)^4$. Thus, in order that $\chi_{O,\text{approx}}$ and χ_O differ by order $(\Delta\tau)^2$, it is sufficient that

$$\langle O(\tau_l)O\rangle_{\text{approx}}-\langle O(\tau_l)O\rangle=\text{order}(\Delta\tau)^2 \tag{B15}$$

for $\Delta\tau$ small, where τ is here limited to the values $l(\Delta\tau), l=0,\ldots,L-1$.

If $\langle D(\beta)\rangle$ vanishes, as was shown previously, we find that

$$\langle O(\tau_l)O\rangle_{\text{approx}}-\langle O(\tau_l)O\rangle =(\Delta\tau)\left[\left\langle O(\tau)\int_0^\tau d\tau' C(\tau')O\right\rangle +\left\langle O(\beta-\tau)\int_0^{\beta-\tau}d\tau' C(\tau')O\right\rangle\right] +\text{order}(\Delta\tau)^2 . \tag{B16}$$

If the operator O either remains the same or changes sign under the interchange of up and down spin labels, the previous reasoning applied to $\langle O(\tau_l)O\rangle_{\text{approx}}$ tells us that this linear term in $\Delta\tau$ vanishes. Thus, for all spin and charge correlations and susceptibilities, the error term linear in $\Delta\tau$ vanishes when the Trotter breakup of Eq. (A18) is used, and we can extrapolate in $(\Delta\tau)^2$ as usual.

---

*Current address: Department of Physics, University of California at Santa Barbara, Santa Barbara, CA 93106.

[1]P. A. Lee, T. M. Rice, J. W. Serene, L. J. Sham, and J. W. Wilkins, Comments Cond. Matter Phys. **12**, 99 (1986), and references therein.
[2]M. A. Ruderman and C. Kittel, Phys. Rev. **96**, 99 (1954).
[3]C. Jayaprakash, H. R. Krishnamurthy, and J. W. Wilkins, Phys. Rev. Lett. **47**, 737 (1981).
[4]R. M. Fye, J. E. Hirsch, and D. J. Scalapino, Phys. Rev. B **35**, 4901 (1987), and references therein.
[5]B. A. Jones, C. M. Varma, and J. W. Wilkins, Phys. Rev. Lett. **61**, 125 (1988).
[6]B. A. Jones, B. G. Kotliar, and A. J. Millis, Phys. Rev. B **39**, 3415 (1989). In this work, an externally imposed exchange term between the two impurity spins, $\mathcal{J}\mathbf{S}_1\cdot\mathbf{S}_2$, is explicitly added to the original Hamiltonian of Eq. (1). This is because effects due to the RKKY interaction, which arises naturally from the Hamiltonian of Eq. (1), vanish in the large-N limit; thus, the introduction of such an extra term is necessary.
[7]B. A. Jones, Ph.D. thesis, Cornell University, 1988.
[8]K. G. Wilson, Rev. Mod. Phys. **47**, 773 (1979).
[9]J. E. Hirsch and R. M. Fye, Phys. Rev. Lett. **56**, 2521 (1986).
[10]R. M. Fye and J. E. Hirsch, Phys. Rev. B **38**, 433 (1988).
[11]R. M. Fye, Phys. Rev. B **33**, 6271 (1986).
[12]R. M. Fye and R. T. Scalettar, Phys. Rev. B **36**, 3833 (1987).
[13]J. E. Hirsch, Phys. Rev. B **28**, 4059 (1983).
[14]J. R. Schrieffer and P. A. Wolff, Phys. Rev. **149**, 491 (1966).
[15]F. D. M. Haldane, J. Phys. C **11**, 5015 (1978).
[16]H. R. Krishnamurthy, J. W. Wilkins, and K. G. Wilson, Phys. Rev. B **21**, 1003 (1980).
[17]A. M. Tsvelick and P. B. Wiegmann, Adv. Phys. **32**, 453 (1983), and references therein.
[18]B. Horvatic and V. Zlatic, J. Phys. (Paris) **46**, 1459 (1985).
[19]R. M. Fye and J. E. Hirsch, Phys. Rev. B (to be published).
[20]H. F. Trotter, Proc. Am. Math. Soc. **10**, 545 (1959).
[21]R. Blankenbecler, D. J. Scalapino, and R. L. Sugar, Phys. Rev. D **24**, 2278 (1981).